

## Supporting Information

*for*

### Reversible Pt<sup>II</sup>-CH<sub>3</sub> deuteration without methane loss: metal-ligand cooperation vs ligand-assisted Pt<sup>II</sup>-protonation

Shrinwantu Pal,<sup>\*,1</sup> Kyoko Nozaki,<sup>1</sup> Andrei N. Vedernikov<sup>2</sup> and Jennifer A. Love<sup>3,+\*</sup>

<sup>1</sup>Department of Chemistry and Biotechnology, The University of Tokyo, 7-3-1 Hongo, Bunkyo-ku, Tokyo 113-8656 Japan

<sup>2</sup>Department of Chemistry and Biochemistry, The University of Maryland, College Park, Maryland 20742 USA

<sup>3</sup>Department of Chemistry, The University of British Columbia, Vancouver, British Columbia V6T 1Z1, Canada

<sup>+</sup>*Current Address:* Department of Chemistry, The University of Calgary, 2500 University Dr. NW, Calgary, Alberta T2N 1N4 Canada.

---

#### Contents:

1. General Procedures
2. Synthesis and Characterization of compounds
3. Mechanistic Analysis and Diagnostic NMR spectra
4. Details of X-ray crystallographic characterization of complex **8**
5. Computational details and free energy tables
6. References

---

Molecular structures (MOL2) and an archive (ZIP) containing animations (GIF) of imaginary frequencies corresponding to transition states are provided separately

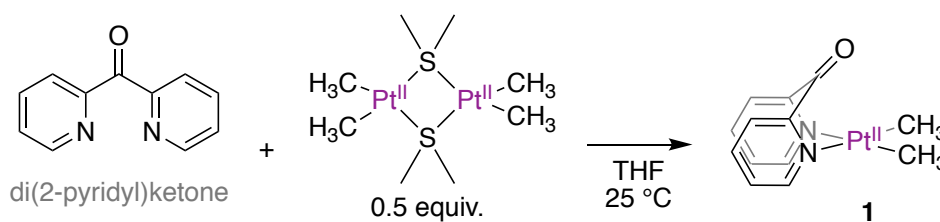
## S1. General Procedures

All manipulations were carried out using standard Schlenk or Glove-box techniques under purified argon using rigorously dried solvents. All NMR analyses were performed in Teflon-capped J. Young NMR tubes.  $^1\text{H}$  and  $^{13}\text{C}$  NMR spectra were recorded on a Bruker Avance 400 or 500 MHz spectrometers. Chemical shifts are reported in ppm and appropriately referenced to the corresponding solvent resonances.<sup>1</sup> “Pt-satellites” and “Pt-shoulders” imply resolved and unresolved doublets, respectively, observed as a result of coupling to the  $^{195}\text{Pt}$  nucleus. Elemental analyses were performed by analytical services at the Department of Chemistry of the University of British Columbia. ESI-MS (high resolution and low resolution) recorded on a JEOL AccuTOF LC-plus (JMS T100LP) instrument were compared with isotopic mass envelopes, and the most-intense peaks are reported. All reagents for which syntheses are not given are commercially available and were used as received without further purification.  $[(\text{CH}_3)_2\text{Pt}^{\text{II}}(\mu\text{-SMe}_2)]_2$  was prepared as previously reported.<sup>2</sup> 99.8%-deuterated  $\text{CD}_3\text{OD}$  or  $\text{CD}_3\text{OH}$  (Sigma-Aldrich) were used for H/D exchange experiments.

## S2. Synthesis and characterization of compounds

### S2.1. $\text{DPKPt}^{\text{II}}(\text{CH}_3)_2$ , complex **1**:

Complex **1** was synthesized as previously reported<sup>3</sup> from 220.2 mg (1.2 mmol) DPK and 343.1 mg  $[(\text{CH}_3)_2\text{Pt}^{\text{II}}(\mu\text{-SMe}_2)]_2$  using ca. 10 mL THF as solvent. Complex **1** was isolated as 450.6 mg of a brick-red colored microcrystalline solid

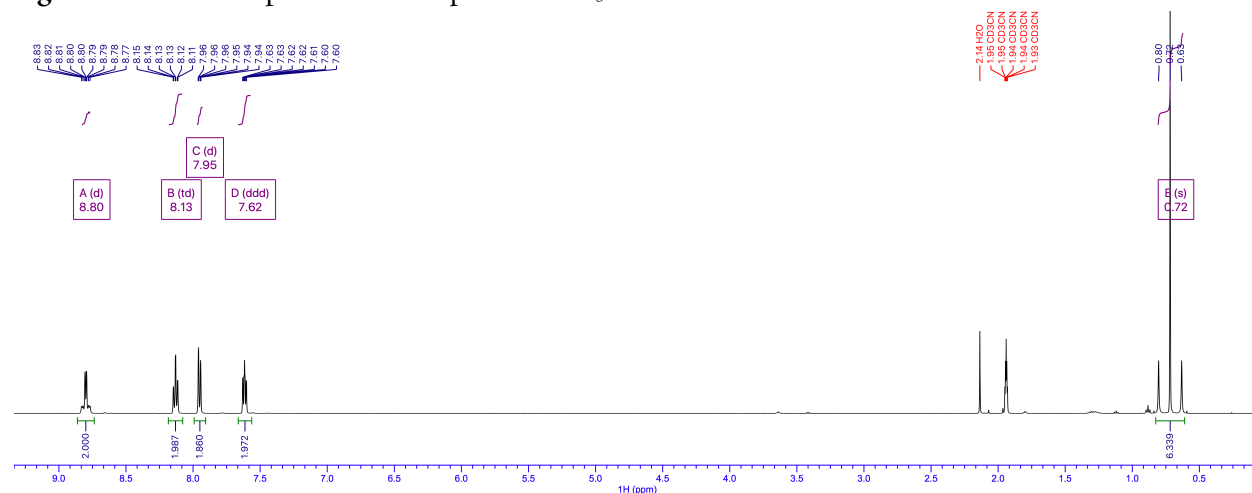


in 92% yield. The  $^1\text{H}$  and  $^{13}\text{C}$  NMR spectra are being provided below for reference purposes.

$^1\text{H}$  NMR (25 °C, 500.15 MHz,  $\text{CD}_3\text{CN}$ , ppm)  $\delta$ : 8.80 (d+Pt-satellites,  $J_{\text{H-H}} = 5.0$  Hz,  $^3J_{\text{Pt-H}} = 26.3$  Hz, 2H, py-6-CH), 8.13 (td,  $J_{\text{H-H}} = 7.8$ , 1.6 Hz, 2H, py-4-CH), 7.95 (d,  $J_{\text{H-H}} = 7.9$  Hz, 2H, py-3-CH), 7.62 (ddd,  $J_{\text{H-H}} = 7.4$ , 5.5, 1.5 Hz, 2H, py-5-CH), 0.72 (s+Pt-satellites,  $^3J_{\text{Pt-H}} = 85.9$  Hz, 6H,  $\text{Pt}^{\text{II}}\text{CH}_3$ )

$^{13}\text{C}$  NMR (25 °C, 125.78 MHz,  $\text{CD}_3\text{CN}$ , ppm)  $\delta$ : 190.06 (C=O), 154.37 (py), 151.14 ( $J_{\text{Pt-C}} = 16.9$  Hz, py), 138.95, 129.52 ( $J_{\text{Pt-C}} = 24.8$  Hz, py), 126.13 ( $J_{\text{Pt-C}} = 12.0$  Hz, py), -16.77 ( $^1J_{\text{Pt-C}} = 829.6$  Hz,  $\text{Pt}^{\text{II}}\text{CH}_3$ )

Figure S1.  $^1\text{H}$  NMR spectrum of complex **1** in  $\text{CD}_3\text{CN}$





glass frit (fine) to remove unreacted sodium hydride directly into a 50 mL screw-cap vial equipped with a stir-bar. The contents of the vial and the frit were washed with an additional 20 mL THF (10 mL x 2 fractions). The screw-cap vial was capped with a Teflon-coated septum and taken out the glove-box and 110  $\mu$ L methyl iodide (1.1. equiv.) was added via a gas-tight microliter syringe. The reaction mixture immediately assumed a green-brown color. The reaction mixture was stirred in the screw-capped vial for 6 hours during which the mixture became orange in color. No precipitation was observed. The contents were opened to air and the solution carefully transferred into an Erlenmeyer flask containing 100 mL dichloromethane. Immediately, copious amounts of a white precipitate formed. The mixture was transferred to a separatory funnel and the organic layer was washed with brine to remove inorganic impurities (e.g. sodium iodide). The organic layer was dried over anhydrous sodium sulfate (once again, use of anhydrous magnesium sulfate was found to be detrimental to yields) and dried under dynamic high vacuum to obtain 305 mg of 2,2'-(1-methoxyethane-1,1-diyl)dipyridine as a yellow colored oil in 89% yield. The crude ligand was used *as-is* for the synthesis of complex **2**.

**<sup>1</sup>H NMR** (25 °C, 500.15 MHz, CDCl<sub>3</sub>, ppm)  $\delta$ : 8.66 (m, 2H, py-6-CH), 7.64 (vt,  $J_{H-H}$  = 7.8 Hz, 2H, py-4-CH), 7.56 (vd,  $J_{H-H}$  = 7.8 Hz, py-3-CH), 7.12 (ddd,  $J_{H-H}$  = 4.95, 4.95, 1.4 Hz, 2H, py-5-CH), 3.25 (s, 3H, OCH<sub>3</sub>), 2.05 (s, 3H, CH<sub>3</sub>)

**<sup>13</sup>C NMR** (25 °C, 125.78 MHz, CDCl<sub>3</sub>, ppm)  $\delta$ : 163.98 (py), 148.87 (py), 136.49 (py), 122.00 (py), 121.20 (py), 83.66 (py<sub>2</sub>C(OCH<sub>3</sub>))(CH<sub>3</sub>), 51.21 (OCH<sub>3</sub>), 22.32 (CH<sub>3</sub>)

ESI-MS: Calculated for C<sub>13</sub>H<sub>14</sub>N<sub>2</sub>O: 214.1; Found 214.1

**GCMS:** Analysis was performed with Shimadzu GCMS-QP2010 Ultra gas chromatograph mass spectrometer equipped with InertCap SMS/Sil capillary column (GL Sciences, 30 m  $\times$  0.25 mm, 0.25  $\mu$ m) and electron ionization quadrupole mass spectrometer with helium as carrier gas. The column temperature was controlled as follows: 50 °C for 2 min, 10 °C/min to 300 °C for 3 min. 2,2'-(1-methoxyethane-1,1-diyl)dipyridine was observed at a retention time of 16.2 min, with mass fragments ( $m/z$ ) = 199 [(py<sub>2</sub>C(OCH<sub>3</sub>))] <sup>+</sup>, 184 [(py<sub>2</sub>C(CH<sub>3</sub>))] <sup>+</sup>, 136 [(pyC(CH<sub>3</sub>)(OCH<sub>3</sub>))] <sup>+</sup>.

**Figure S3.** <sup>1</sup>H NMR spectrum of 2,2'-(1-methoxyethane-1,1-diyl)dipyridine in CDCl<sub>3</sub>

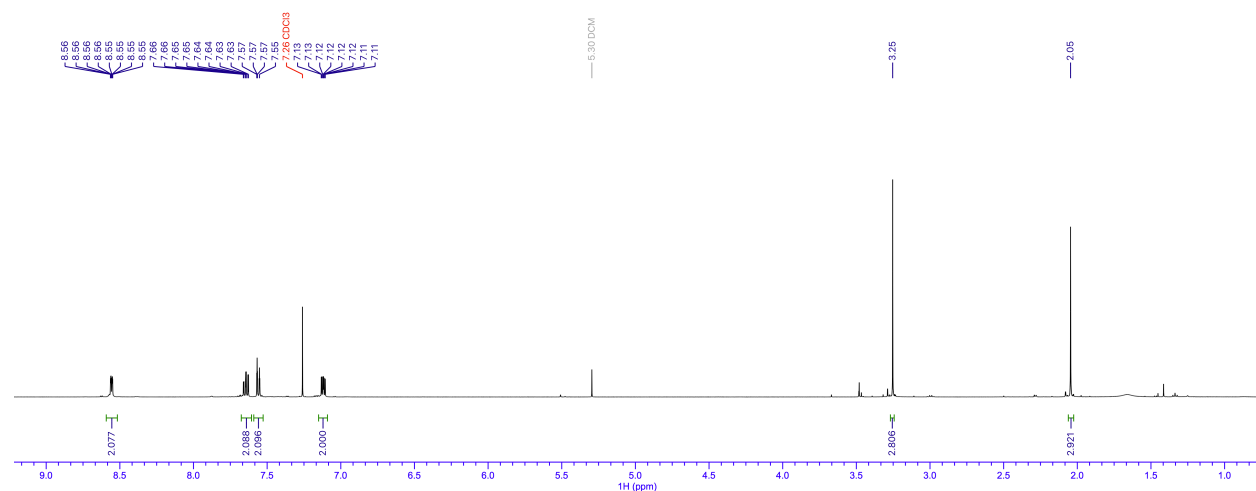
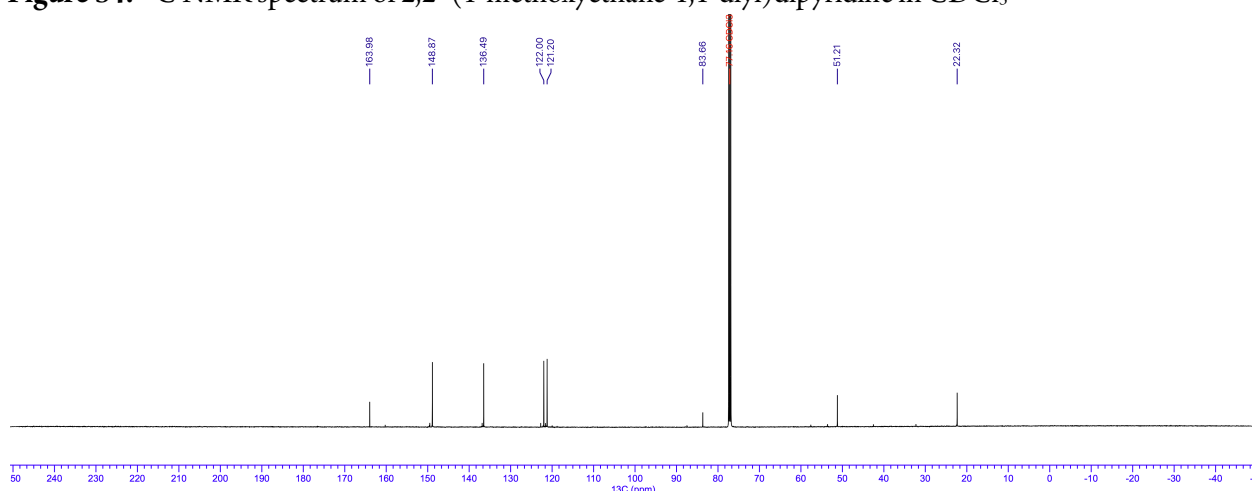
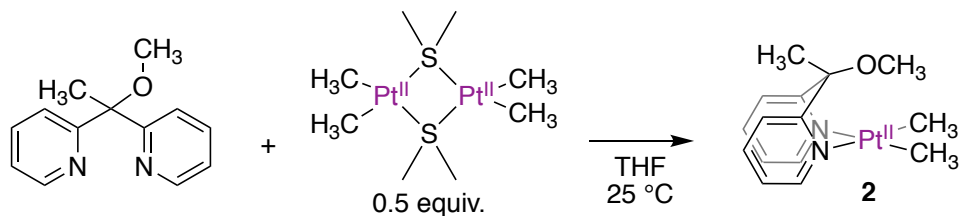


**Figure S4.**  $^{13}\text{C}$  NMR spectrum of 2,2'-(1-methoxyethane-1,1-diyl)dipyridine in  $\text{CDCl}_3$



• **Synthesis of 2,2'-(1-methoxyethane-1,1-diyl)dipyridine dimethylplatinum(II), complex 2:**

120 mg (560  $\mu\text{mol}$ ) 2,2'-(1-methoxyethane-1,1-diyl)dipyridine was dissolved in ca. 3 mL THF in a vial in the glove box. In a separate vial equipped with a stir-bar, 161 mg (280  $\mu\text{mol}$ )  $[(\text{CH}_3)_2\text{Pt}^{\text{II}}(\mu\text{-SMe}_2)]_2$  was weighed out and dissolved in ca. 2 mL THF. The solution of the ligand was added to the vial containing the Pt-precursor with



stirring. An additional ca. 3 ml (1.5 mL x 2 times) was used to ensure quantitative transfer of the ligand. After completion of addition, a homogenous yellow colored solution resulted. The solution was stirred for a period of 8 hours and exposed to dynamic vacuum to facilitate removal of  $\text{SMe}_2$ . After the volume reduced to  $\sim 2$  mL, the resulting oily yellow-orange liquid was layered with ether and stored at  $-35$   $^\circ\text{C}$ . Large yellow colored crystals (suitable for X-ray diffraction) were obtained. The supernatant was carefully decanted and the crystals were collected and dried to afford 209.5 mg of complex **2** as an analytically pure yellow solid in 85 % yield. An additional crop ( $\sim 20$  mg) recovered from the supernatant was found to also contain the target product; however, contaminated with free ligand and other byproducts. Since the yield from the first recrystallization was satisfactory, further attempts to recover complex **2** from the supernatant were not made.

$^1\text{H}$  NMR (25  $^\circ\text{C}$ , 500.15 MHz,  $\text{THF-}d_8$ , ppm)  $\delta$ : 8.92 (d+Pt-shoulders,  $J_{\text{H-H}} = 5.5$  Hz,  $J_{\text{Pt-H}} \sim 27$  Hz, 2H, py-6-CH), 7.93 (vt,  $J_{\text{H-H}} = 6.2$  Hz, 2H, py-CH), 7.82 (d,  $J_{\text{H-H}} = 7.9$  Hz, 2H, py-3-CH), 7.22 (m, 2H, py-4-CH), 3.68 (br, 3H,  $\text{OCH}_3$ ), 3.13 (br, 3H,  $\text{CH}_3$ ), 0.78 (s+Pt-satellites,  $^2J_{\text{Pt-H}} = 86.8$  Hz,  $\text{Pt}^{\text{II}}\text{-CH}_3$ )

$^{13}\text{C}$  NMR (25  $^\circ\text{C}$ , 125.78 MHz,  $\text{THF-}d_8$ , ppm)  $\delta$ : 161.2 (s, py-2-C), 151.6 (s+Pt-satellites,  $J_{\text{Pt-C}} = 21.6$  Hz, py), 136.9 (py), 124.8 (s+Pt-satellites,  $J_{\text{Pt-C}} = 24.2$  Hz, py), 122.5 (py), 85.8 ( $\text{C}(\text{CH}_3)(\text{OCH}_3)$ ), 52.5 (br,  $\text{C}(\text{CH}_3)(\text{OCH}_3)$ ), 20.48 (br,  $\text{C}(\text{CH}_3)(\text{OCH}_3)$ ),  $-18.51$  (s+Pt-satellites,  $^1J_{\text{Pt-C}} = 858.6$  Hz,  $\text{Pt}^{\text{II}}\text{-CH}_3$ )

**Elemental Analysis** (C, H, N): Calculated: 41.00, 4.59, 6.38; Found: 40.97, 4.68, 6.55

**Figure S5.**  $^1\text{H}$  NMR spectrum of complex **2** in  $\text{THF-}d_8$

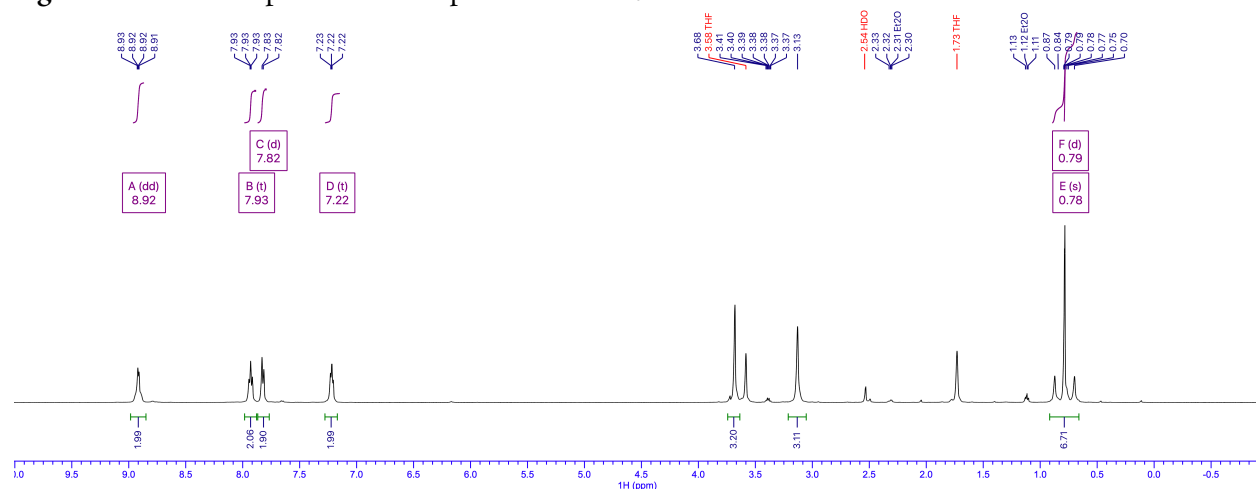


**Figure S6.**  $^{13}\text{C}$  NMR spectrum of complex **2** in  $\text{THF-}d_8$

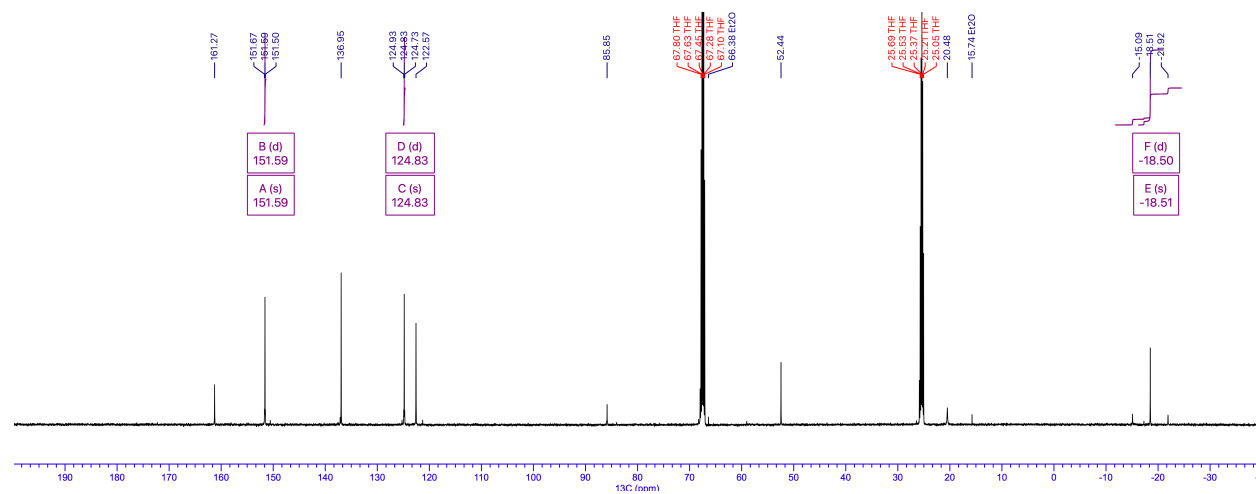
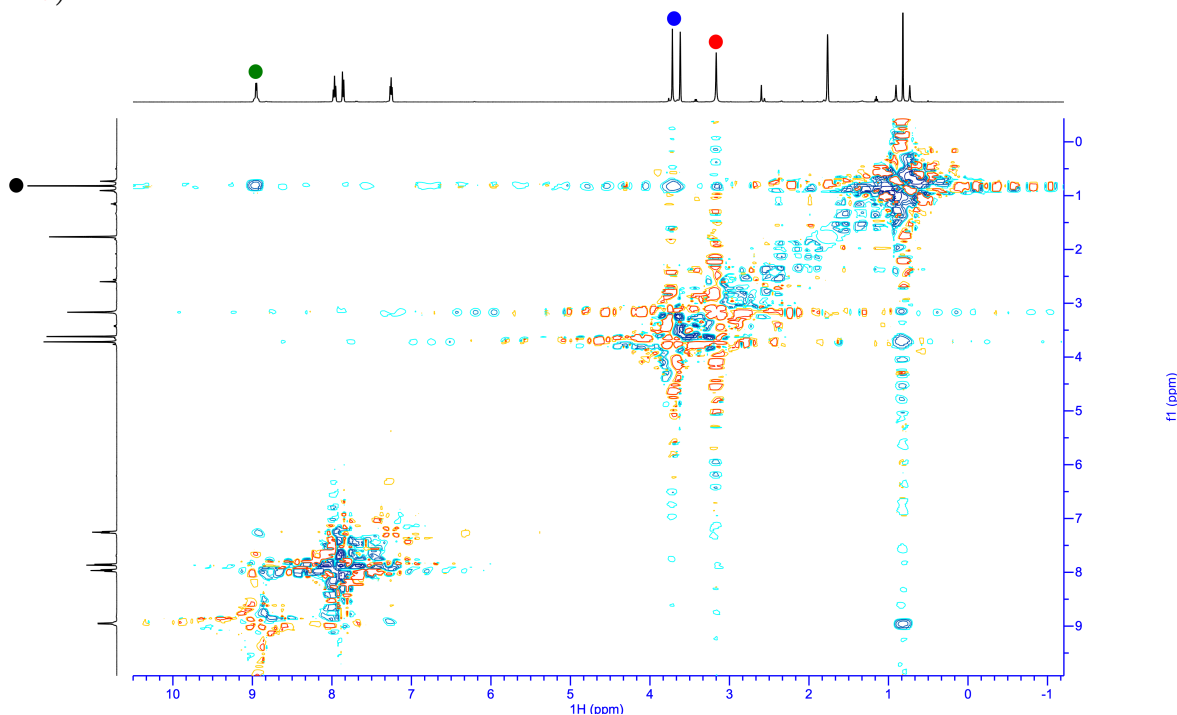
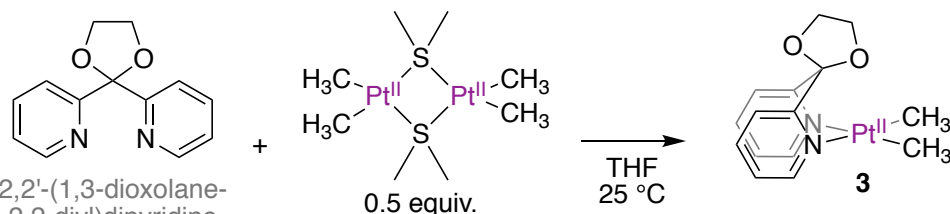


**Figure S7.** 2D  $^1\text{H}$  NOE NMR spectrum of complex **2** in  $\text{THF-}d_8$  showing correlation of the  $\text{Pt}^{\text{II}}\text{-CH}_3$  resonances (black circle ●) with py-6-CH (green circle ●),  $\text{py}_2\text{C}(\text{OCH}_3)$  (blue circle ●) and  $\text{py}_2\text{C}(\text{CH}_3)$  (red circle ●)



### S2.3. Synthesis of Complex 3:

2,2'-(1,3-dioxolane-2,2-diyl)dipyridine ligand was prepared by the procedure reported.<sup>4</sup> Complex **3** was synthesized using a synthetic procedure identical to that used for complex **2** using 125 mg (547  $\mu\text{mol}$ ) of 2,2'-(1,3-dioxolane-2,2-diyl)dipyridine



and 157.5 mg (274  $\mu\text{mol}$ ) of  $[(\text{CH}_3)_2\text{Pt}^{\text{II}}(\mu\text{-SMe}_2)]_2$ . After trituration with ether and storage at  $-35\text{ }^\circ\text{C}$  overnight, 201 mg of complex **3** was obtained as a yellow microcrystalline analytically pure solid in 81% yield.

$^1\text{H}$  NMR (25  $^\circ\text{C}$ , 400.2 MHz,  $\text{CDCl}_3$ , ppm)  $\delta$ : 8.39 (d+Pt-satellites,  $J_{\text{H-H}} = 5.6$  Hz,  $^3J_{\text{Pt-H}} = 24.5$  Hz, 2H, py-6-CH), 7.3-7.2 (m, 4H, overlapping with  $\text{CDCl}_3$ ), 6.67-6.6 (m, 2H, py-5-CH), 3.67 (t,  $J_{\text{H-H}} = 6$  Hz, 2H,  $\text{CH}_2$ ), 3.46 (t,  $J_{\text{H-H}} = 6$  Hz, 2H,  $\text{CH}_2$ ), 0.33 (s+Pt-satellites,  $^2J_{\text{Pt-H}} = 84.5$  Hz, 6H,  $\text{Pt}^{\text{II}}\text{-CH}_3$ )

$^{13}\text{C}$  NMR (25  $^\circ\text{C}$ , 100.64 MHz,  $\text{CDCl}_3$ , ppm)  $\delta$ : 155.24, 151.32 (s+Pt-satellites,  $J_{\text{Pt-C}} = 21.33$  Hz), 136.4, 125.67 (s+Pt-satellites,  $J_{\text{Pt-C}} = 24.2$  Hz), 122.08, 108.25 ( $\text{Py}_2\text{C}$ ), 66.60 ( $\text{OCH}_2$ ), 65.93 ( $\text{OCH}_2$ ), -19.20 (s+Pt-satellites,  $^1J_{\text{Pt-C}} = 831$  Hz,  $\text{Pt}^{\text{II}}\text{-CH}_3$ )

**Elemental Analysis** (C, H, N): Calculated: 39.74, 4.00, 6.18; Found: 39.66, 4.10, 6.38

Figure S8.  $^1\text{H}$  NMR spectrum of complex 3 in  $\text{CDCl}_3$

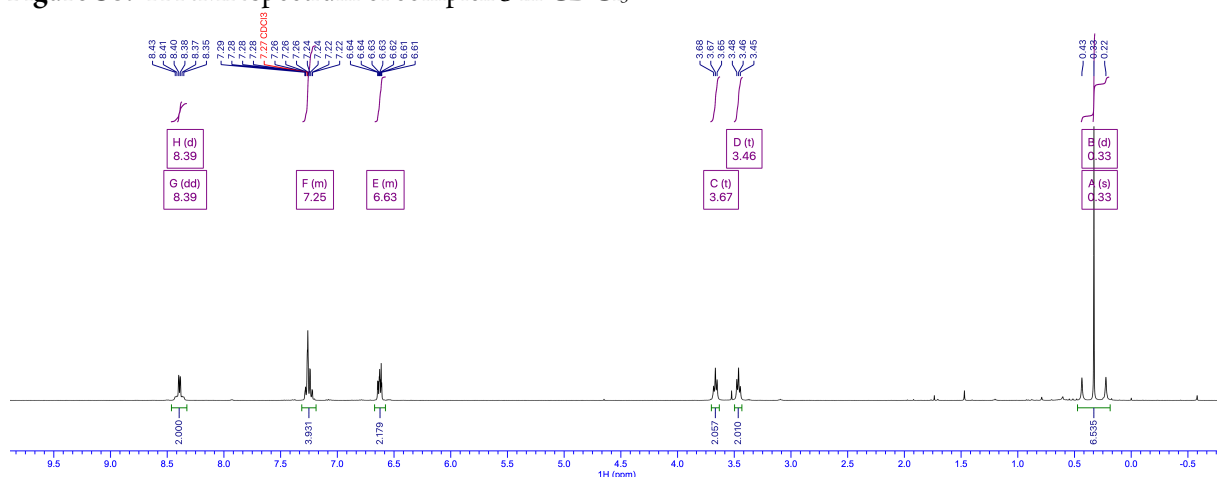


Figure S9.  $^{13}\text{C}$  NMR spectrum of complex 3 in  $\text{CDCl}_3$

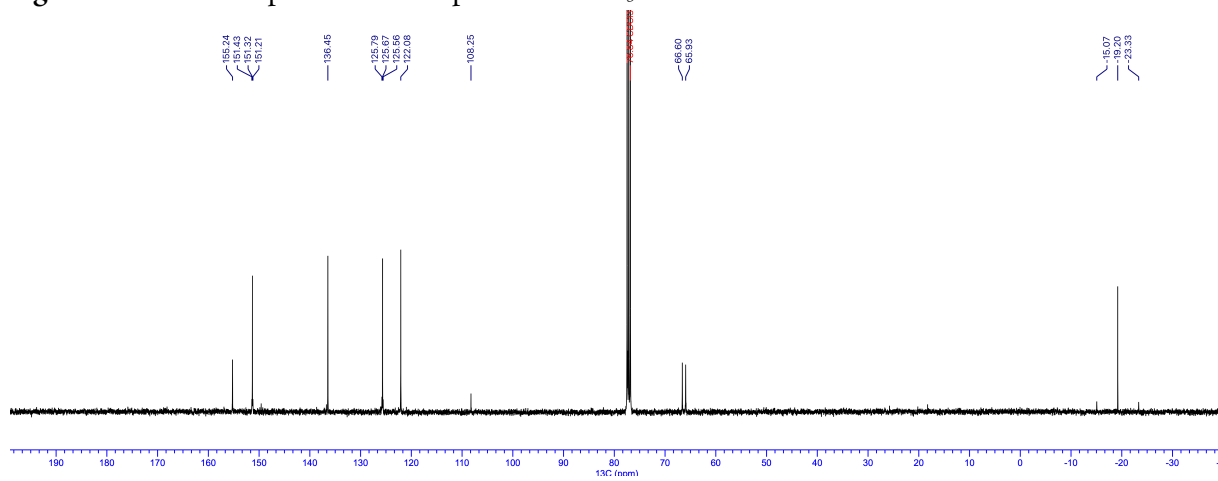
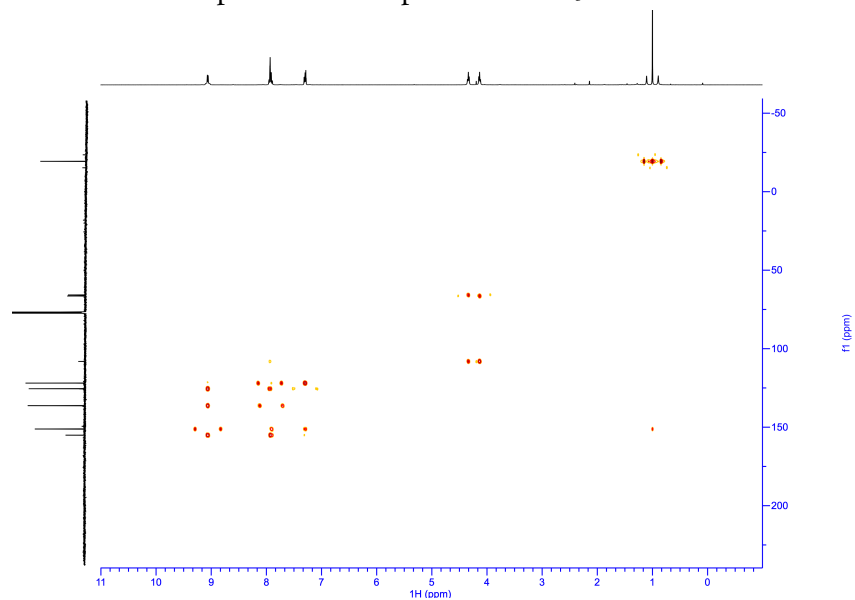
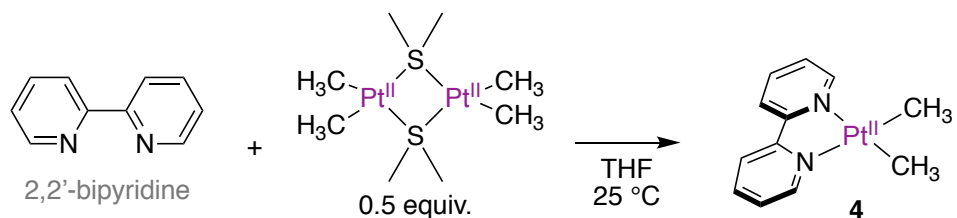


Figure S10.  $^1\text{H}$ - $^{13}\text{C}$  HMBC NMR spectrum of complex 3 in  $\text{CDCl}_3$

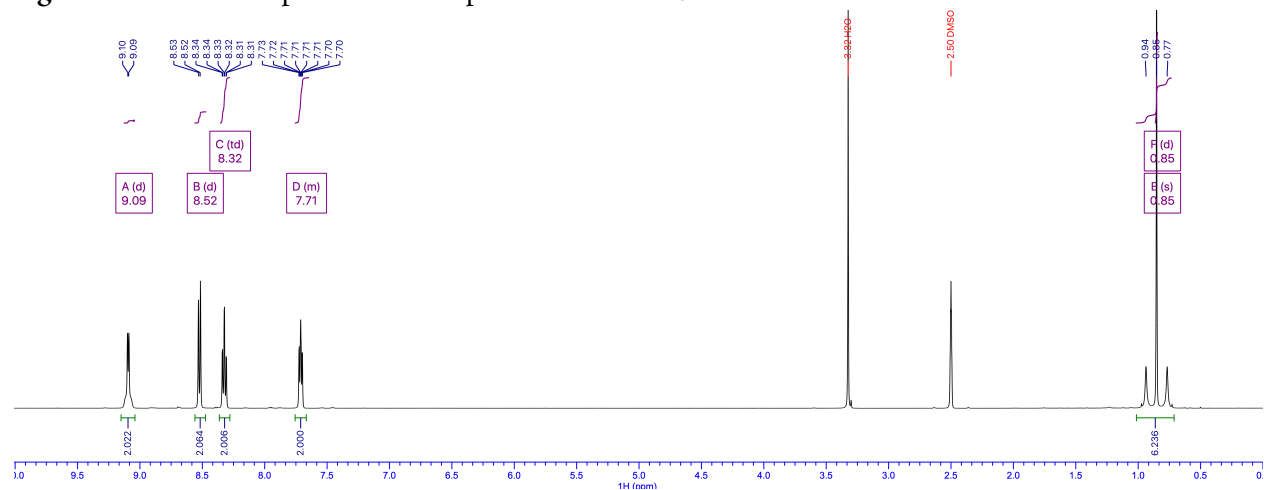


**S2.4. Synthesis of Complex 4:** Synthesis of complex **4** was performed as previously reported<sup>5</sup> using 50 mg of 2,2'-bipyridine (320  $\mu\text{mol}$ ) and 92 mg  $[(\text{CH}_3)_2\text{Pt}^{\text{II}}(\mu\text{-SMe}_2)]_2$ . The  $^1\text{H}$  NMR spectrum of was identical to that reported and being provided below for reference purposes. Complex **4** was found to be stable in  $\text{DMSO-}d_6$  solution at 25  $^\circ\text{C}$  for at least a weak under air-free conditions.



$^1\text{H NMR}$  (25  $^\circ\text{C}$ , 500.15 MHz,  $\text{DMSO-}d_6$ , ppm)  $\delta$ : 9.09 (d+Pt-shoulders,  $J_{\text{H-H}} = 5.4 \text{ Hz}$ ,  $^3J_{\text{Pt-H}} \sim 22 \text{ Hz}$ , 2H, py-6-CH), 8.52 (d,  $J_{\text{H-H}} = 8.2 \text{ Hz}$ , 2H, py-3-CH), 8.32 (td,  $J_{\text{H-H}} = 7.8, 1.4 \text{ Hz}$ , 2H, py-5-CH), 7.71 (m, 2H, py-4-CH), 0.85 (s+Pt-satellites,  $^2J_{\text{Pt-H}} = 85.5 \text{ Hz}$ , 6H,  $\text{Pt}^{\text{II}}\text{-CH}_3$ )

**Figure S11.**  $^1\text{H NMR}$  spectrum of complex **4** in  $\text{DMSO-}d_6$



-----End of Section 2-----

## S3. Mechanistic Studies

### S3.1 Reaction of complex **1** with CD<sub>3</sub>OD:

**In situ monitoring:** 8 mg of **1** was dissolved in 0.6 mL chilled CD<sub>3</sub>OD (stored at -35 °C) in the glove-box and transferred into a J. Young NMR tube. The resulting orange-red solution was analyzed by NMR spectroscopy. Kinetic Analysis (*vide infra*) were performed using similarly prepared solutions.

**<sup>1</sup>H NMR** (25 °C, 500.15 MHz, CD<sub>3</sub>OD, ppm) spectrum recorded ~ 5 minutes after dissolution. THF was used as internal standard for kinetic analysis.  $\delta$ : 8.83 (dd+Pt-satellites,  $J_{H-H} = 5.5, 0.8$  Hz,  $^3J_{Pt-H} = 25.4$  Hz, 2H, py-6-CH), 8.19 (td,  $J_{H-H} = 7.8, 1.6$  Hz, 2H, py-4-CH), 8.04 (ddd,  $J_{H-H} = 7.9, 1.5, 0.8$  Hz, 2H, py-3-CH), 7.68 (ddd,  $J_{H-H} = 7.7, 5.5, 1.5$  Hz, 2H, py-5-CH), 0.78 (s+Pt-satellites,  $^3J_{Pt-H} = 84.6$  Hz, 6H, Pt<sup>II</sup>-CH<sub>3</sub>). Only trace Pt-CH<sub>3</sub> deuteration incorporation observed.  $\delta$ : Pt<sup>II</sup>-CH<sub>3</sub> (0.78 ppm, s), Pt<sup>II</sup>-CH<sub>2</sub>D (0.77 ppm, t), Pt<sup>II</sup>-CHD<sub>2</sub> (0.75 ppm, p) with corresponding Pt-satellites,  $^3J_{Pt-H} = 84.6$  Hz.

**<sup>13</sup>C NMR** (25 °C, 125.78 MHz, CD<sub>3</sub>OD, ppm) spectrum recorded ~ 5 h after dissolution  $\delta$ : 190.06 (C=O), 154.5 (py), 151.34 ( $J_{Pt-C} = 18.4$  Hz, py), 139.38 (py), 129.73 ( $J_{Pt-C} = 24$  Hz, py), 126.59 (py).

**Figure S12.** <sup>1</sup>H NMR spectrum of complex **1-d<sub>n</sub>** in CD<sub>3</sub>OD. Inset (Pt<sup>II</sup>-CH<sub>3-n</sub>D<sub>n</sub> region, ~2 h after dissolution)

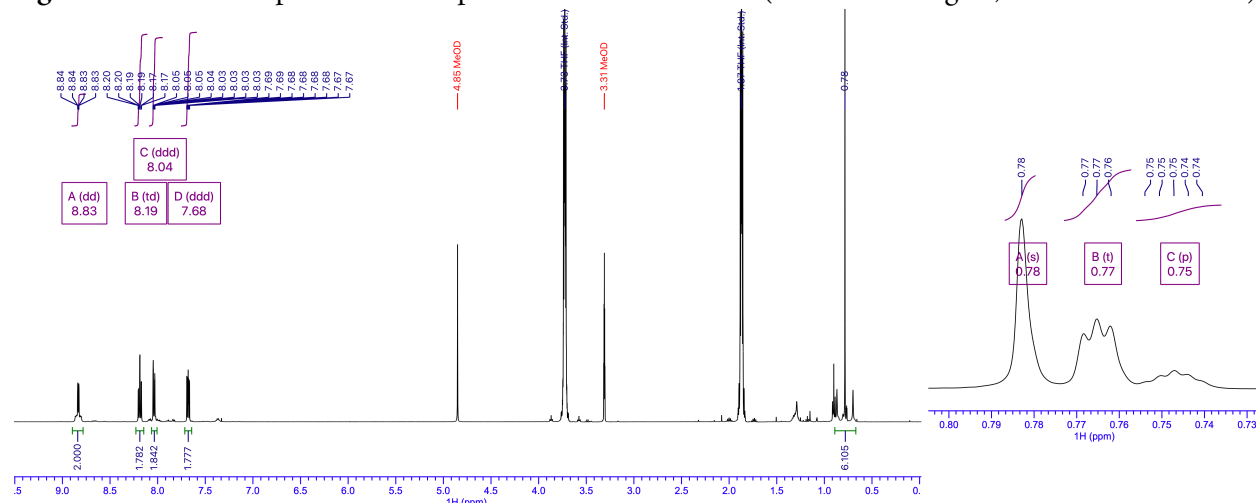
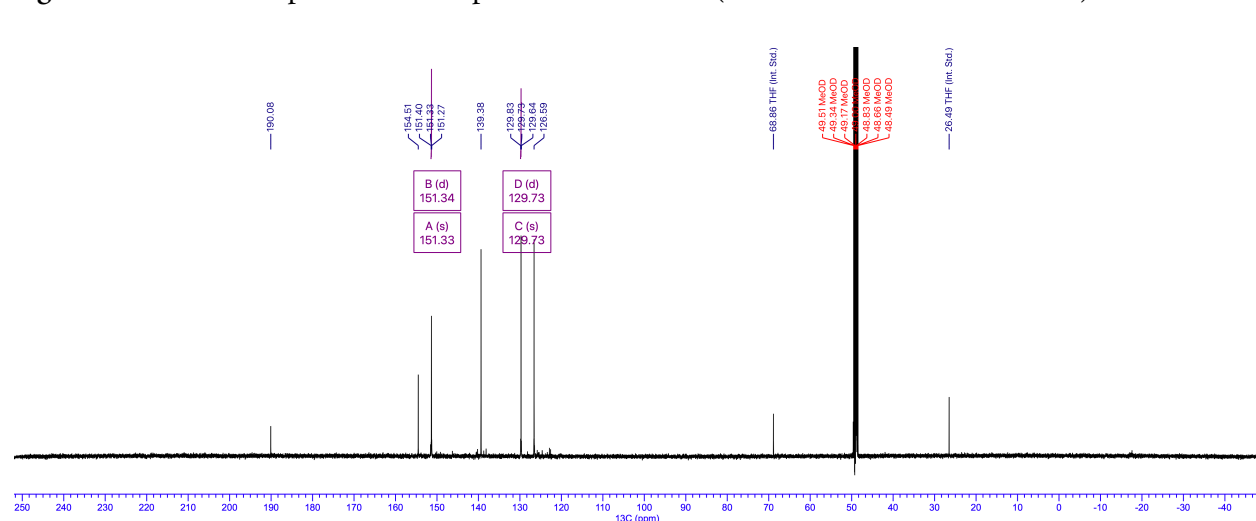


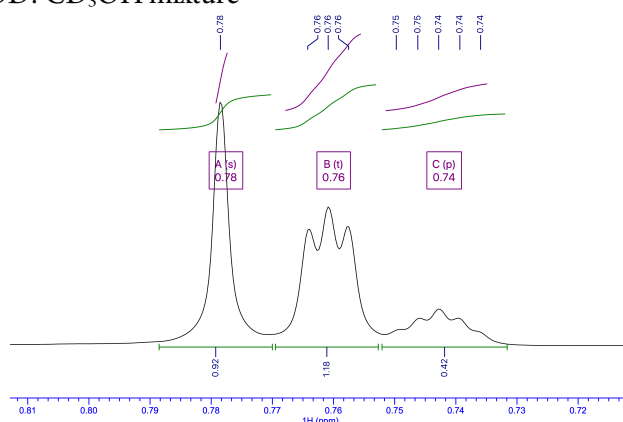
**Figure S13.** <sup>13</sup>C NMR spectrum of complex **1-d<sub>6</sub>** in CD<sub>3</sub>OD (recorded ~5 h after dissolution)



### Determination of equilibrium isotope distribution:

8.0 mg of complex **1** was dissolved in 0.60 mL 1:1 v/v CD<sub>3</sub>OD : CD<sub>3</sub>OH mixture (prepared by mixing 0.30 mL CD<sub>3</sub>OD and 0.30 mL CD<sub>3</sub>OH (essentially 1 : 1 molar ratio)). Calculations based on density and molar mass give 12.31 M and 12.36 M for the individual concentrations, respectively (see Table S1 in the Computational Section). The resulting 33 mM solution of the complex was allowed to stand for 24 h and analyzed by <sup>1</sup>H NMR spectroscopy. Figure S14 shows the region of the spectrum corresponding to the <sup>Y</sup>Pt-CH<sub>x</sub>D<sub>3-x</sub> <sup>1</sup>H NMR resonances ( $x = 1, 2, 3$ ;  $Y \neq 195$ ). The integral intensity of the pyridine signals was set to 2. No changes in the integral intensity ratio was observed after this time. The well-resolved peaks corresponding to the <sup>Y</sup>Pt-CH<sub>x</sub>D<sub>3-x</sub> <sup>1</sup>H NMR signals (i.e., not considering poorly resolved <sup>195</sup>Pt satellites) were used for calculation. The integral intensity ratios for the <sup>Y</sup>Pt-CH<sub>x</sub>D<sub>3-x</sub> signals ( $x = 1, 2, 3$ ) were found to be: Pt-CH<sub>3</sub> : Pt-CH<sub>2</sub>D : Pt-CHD<sub>2</sub> = 0.92 : 1.18 : 0.42, which corresponds to the relative molar concentrations 0.92/3 : 1.18/2 : 0.42/1 = 1 : 1.92 : 1.37. Using <sup>1</sup>H NMR integration of the resulting signals, the equilibrium constants for reactions (1) and (2) were calculated as 0.64 and 0.72 (as shown below), and the corresponding reaction Gibbs energies are 0.26 and 0.20 kcal/mol, respectively, which are in reasonable agreement of the DFT-calculated values of 0.24 and 0.18 kcal/mol, respectively (see Table S2 in the Computational Section).

**Figure S14.** Pt<sup>II</sup>-CH<sub>3-n</sub>D<sub>n</sub> region of the <sup>1</sup>H NMR spectrum of complex **1** recorded 24 h after dissolution in a 1:1 (v/v) mixture of CD<sub>3</sub>OD: CD<sub>3</sub>OH mixture



For the reaction (1),

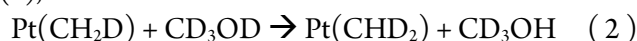


the equilibrium constant is given by:

$$K_{\text{CH}/\text{CD},1} = \frac{[\text{Pt}(\text{CH}_2\text{D})][\text{CD}_3\text{OH}]}{([\text{Pt}(\text{CH}_3)] \times 3)[\text{CD}_3\text{OD}]} = \frac{1.92 \times 12.35}{3 \times 12.30} = 0.64$$

where, the constant is statistically corrected per number of equivalent C-H bonds in the CH<sub>3</sub> ligand involved in equilibrium (1). The corresponding reaction Gibbs energy change is  $\Delta G_{298\text{K}} = -0.593 \times \ln(0.64) = 0.26$  kcal/mol.

Similarly, for the reaction (2),



the equilibrium constant is given by:

$$K_{\text{CH}/\text{CD},2} = \frac{([\text{Pt}(\text{CHD}_2)] \times 2)[\text{CD}_3\text{OH}]}{([\text{Pt}(\text{CH}_2\text{D})] \times 2)[\text{CD}_3\text{OD}]} = \frac{1.37 \times 12.35}{1.92 \times 12.3} = 0.72$$

where, the constant is statistically corrected per number of equivalent C-H bonds CH<sub>2</sub>D ligand and the number of equivalent C-D bonds in the CHD<sub>2</sub> ligand involved in equilibrium (2). The corresponding reaction Gibbs energy change is  $\Delta G_{298K} = -0.593 \cdot \ln(0.72) = 0.20$  kcal/mol.

**Isolation of *1-d<sub>6</sub>*:** 50 mg of **1** was dissolved in 3 mL CD<sub>3</sub>OD in the glove-box and the solution was stirred for a period of 5 hours. After this time, the solution was dried *in vacuo* to obtain 49 mg of a microcrystalline red solid with the same visual appearance as **1** in 96% yield. The product (**1-d<sub>6</sub>**) was analyzed by <sup>1</sup>H and <sup>13</sup>C NMR spectroscopy. The <sup>1</sup>H and <sup>13</sup>C NMR spectra of complex **1-d<sub>6</sub>** are identical to those of complex **1**, except for the absence of the resonances corresponding to the Pt<sup>II</sup>(CD<sub>3</sub>)<sub>2</sub> fragment, as shown below. The NMR spectra of **1-d<sub>6</sub>** in CD<sub>3</sub>OD was found to persist for a week under air-free conditions at 25 °C.

**Figure S15.** <sup>1</sup>H NMR spectrum of complex **1-d<sub>6</sub>** in CD<sub>3</sub>CN

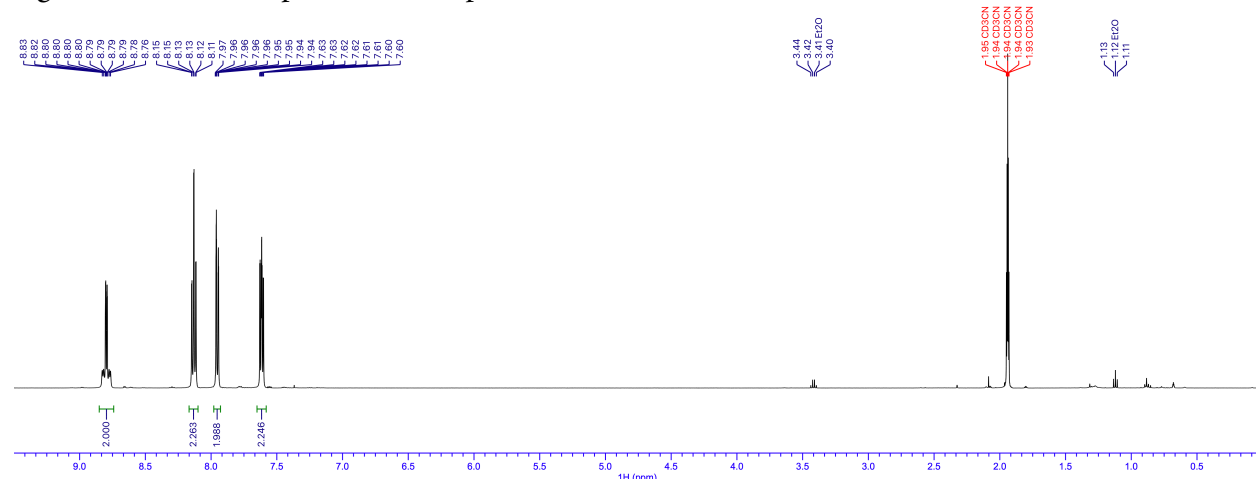
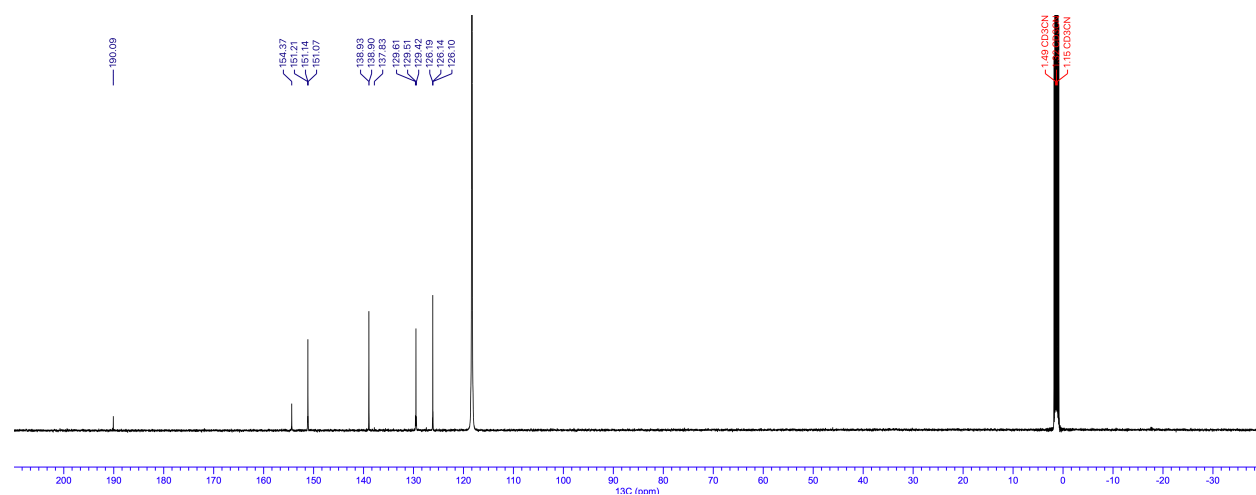
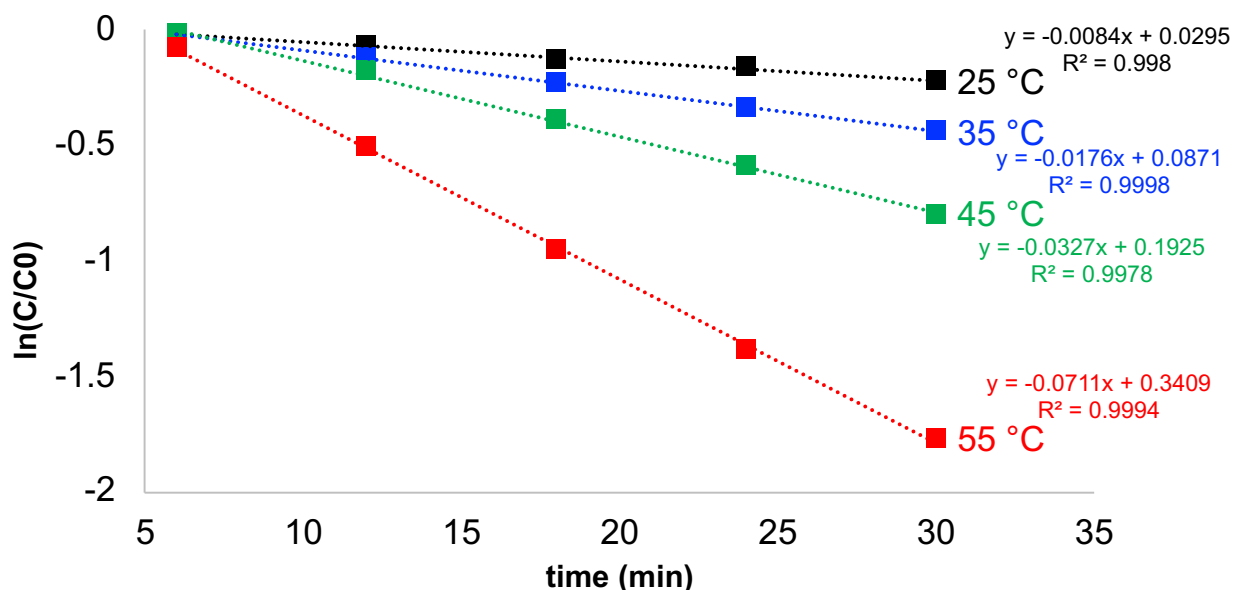


**Figure S16.** <sup>13</sup>C NMR spectrum of complex **1-d<sub>6</sub>** in CD<sub>3</sub>CN



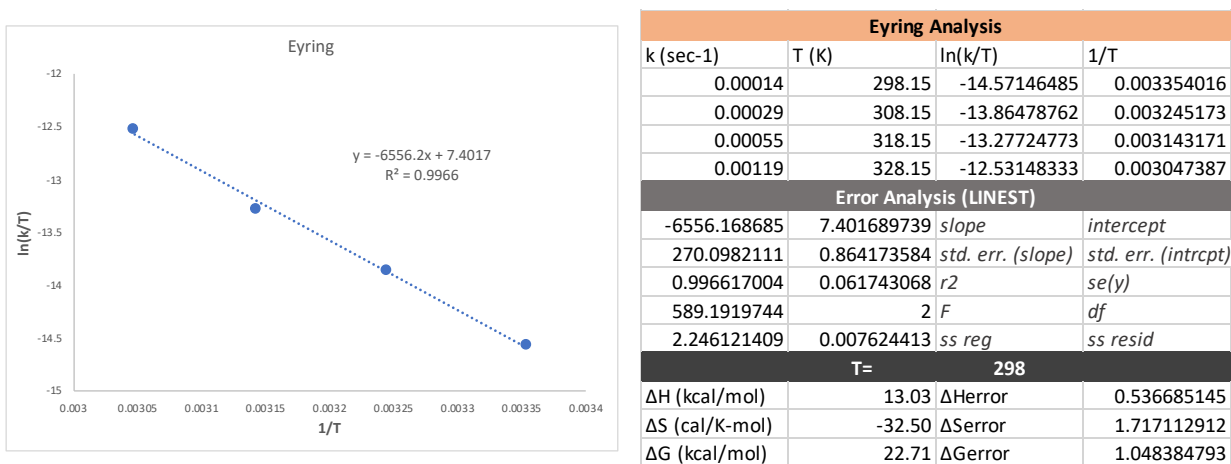
**Eyring Analysis:** CD<sub>3</sub>OD solutions of **1**, prepared as described above, were monitored by <sup>1</sup>H NMR spectroscopy at 25, 35, 45 and 55 °C at intervals of 6 minutes for a period of 30 minutes. The conversion of **1** was measured by integrating the Pt<sup>II</sup>-CH<sub>3</sub> region (0.5-1.0 ppm) with respect to the pyridine C-H fragment (8.8 ppm). Error estimation was performed by the 'LINEST' function within the Microsoft Excel package.

**Figure S17.** Initial rates<sup>†</sup> for the reaction of **1** with CD<sub>3</sub>OD at 25, 35, 45, and 55 °C.



<sup>†</sup>C and C<sub>0</sub> are the total integral intensities of Pt-CH<sub>x</sub>D<sub>3-x</sub> fragments observed in the <sup>1</sup>H NMR spectra at t and t=0 respectively

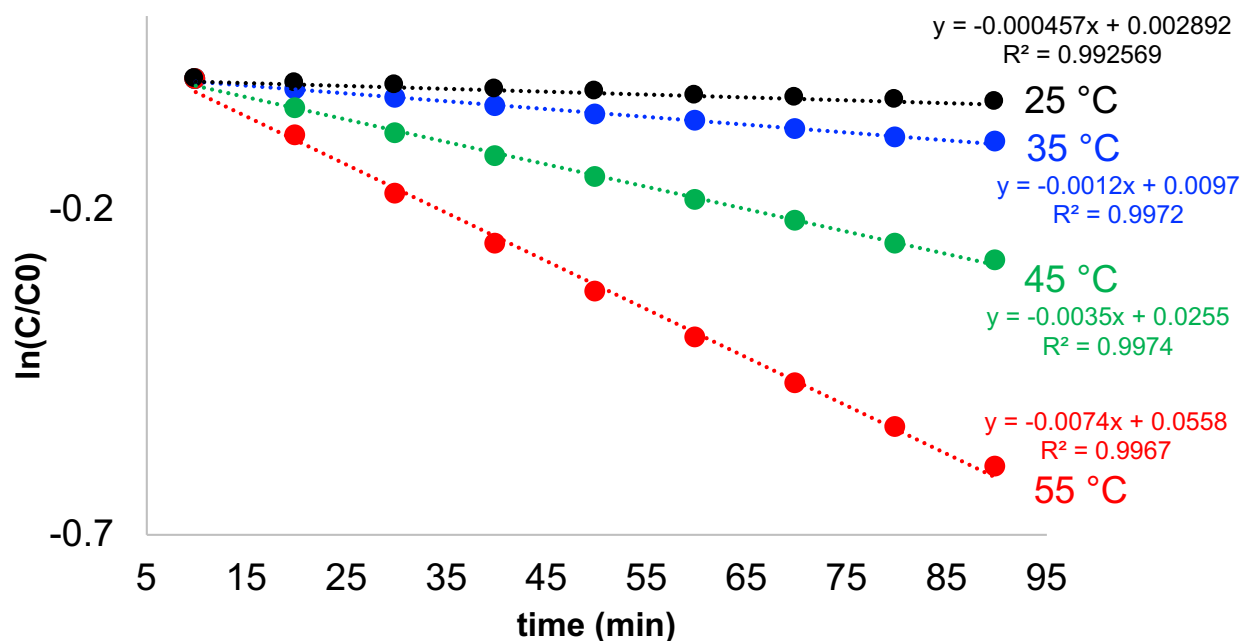
**Figure S18.** Eyring analysis corresponding to the initial rates observed for **1** and error analysis



### S3.2 Reaction of complex **2** with CD<sub>3</sub>OD:

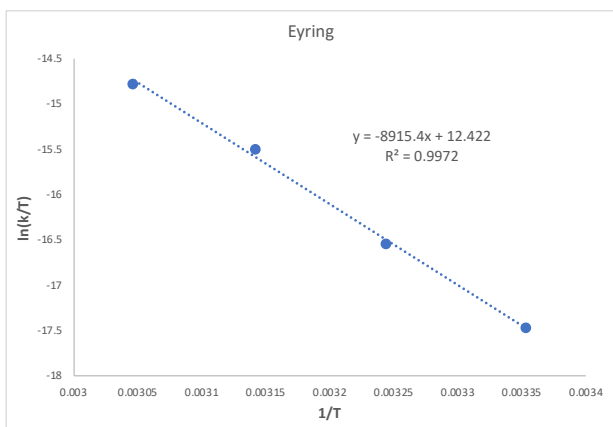
**In situ monitoring:** 4 mg of **2** was dissolved in 0.6 mL CD<sub>3</sub>OD and the solutions were monitored by <sup>1</sup>H NMR spectroscopy at 25, 35, 45 and 55 °C at intervals of 10 minutes for a period of 90 minutes. The conversion of **2** was measured by integrating the Pt<sup>II</sup>-CH<sub>3</sub> region (0.5-1.0 ppm) with respect to the pyridine C-H fragment (8.8 ppm). Error estimation was performed by the 'LINEST' function within the Microsoft Excel package.

**Figure S19.** Initial rates<sup>†</sup> for the reaction of **2** with CD<sub>3</sub>OD at 25, 35, 45, and 55 °C



<sup>†</sup>C and C<sub>0</sub> are the total integral intensities of Pt-CH<sub>x</sub>D<sub>3-x</sub> fragments observed in the <sup>1</sup>H NMR spectra at t and t=0 respectively

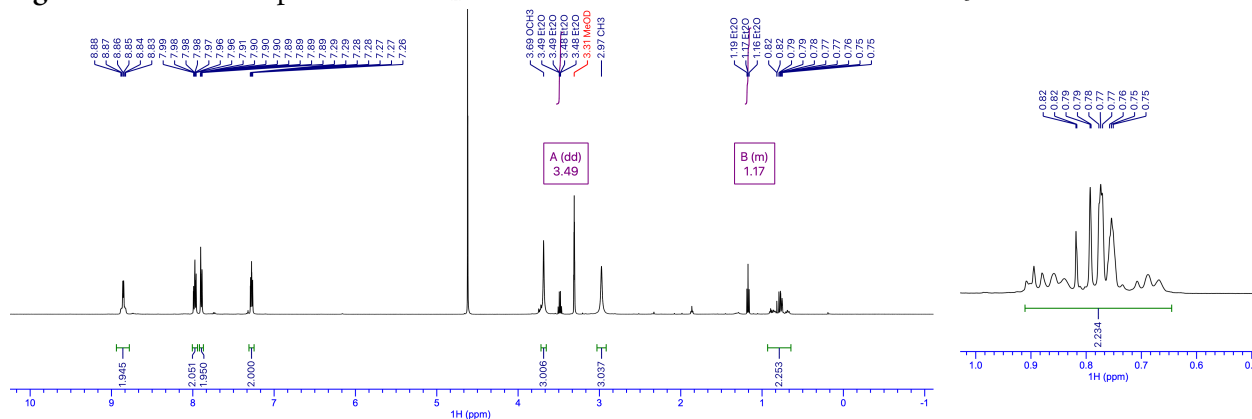
**Figure S20.** Eyring analysis corresponding to the initial rates observed for **2** and error analysis



Eyring Analysis			
k (sec-1)	T (K)	ln(k/T)	1/T
0.00001	298.15	-17.48276844	0.003354016
0.00002	308.15	-16.55036496	0.003245173
0.00006	318.15	-15.51185984	0.003143171
0.00012	328.15	-14.79409066	0.003047387
Error Analysis (LINEST)			
-8915.390548	12.42162766	<i>slope</i>	<i>intercept</i>
335.4758441	1.073347955	<i>std. err. (slope)</i>	<i>std. err. (intrcpt)</i>
0.997176137	0.07668806	<i>r2</i>	<i>se(y)</i>
706.2496357	2	<i>F</i>	<i>df</i>
4.153495406	0.011762117	<i>ss reg</i>	<i>ss resid</i>
T=		298	
ΔH (kcal/mol)	17.71	ΔHerror	0.666590502
ΔS (cal/K-mol)	-22.53	ΔSerror	2.132742387
ΔG (kcal/mol)	24.43	ΔGerror	1.302147733

**Attempted isolation of 2-d<sub>6</sub> from reaction of 2 with CD<sub>3</sub>OD:** The reaction of **2** with CD<sub>3</sub>OD was found to be incomplete even after 3 days at 25 °C, as shown in Figure S21 (ca. 60% deuteration of Pt<sup>II</sup>-CH<sub>3</sub> fragments, inset)

**Figure S21.** <sup>1</sup>H NMR spectrum of **2-d<sub>n</sub>** recorded ~72 h after dissolution of **2** in CD<sub>3</sub>OD

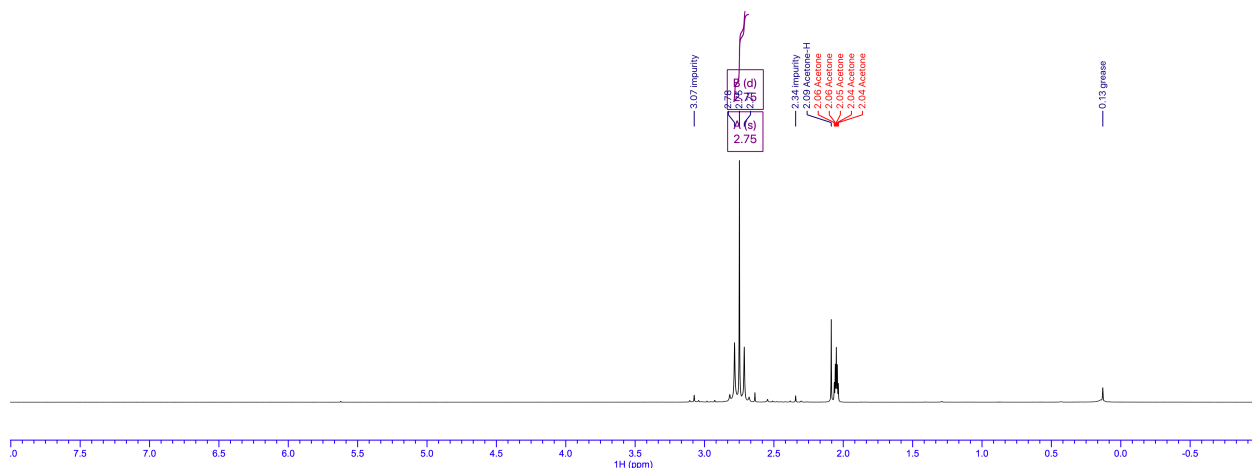


### S3.3 Synthesis of [(CD<sub>3</sub>)<sub>2</sub>Pt<sup>II</sup>(μ-SMe<sub>2</sub>)]<sub>2</sub> and 2-d<sub>6</sub>:

**Synthesis of [(CD<sub>3</sub>)<sub>2</sub>Pt<sup>II</sup>(μ-SMe<sub>2</sub>)]<sub>2</sub>:** 80 mg (122 μmol) complex **1** was dissolved in 4 mL CD<sub>3</sub>OD in a 20 mL screw-capped vial (equipped with a Teflon septum) inside the glove-box and stirred for 5 hours. After this time, the vial was taken out of the glove-box and 180 μL (20 equiv.) dimethylsulfide was added via a gas-tight microliter syringe through the septum. The vial was taken into the glove box and stirred for ~ 3 hours, during the course of which the solution assumed a pale pink color. The solution was layered with 4 mL ether and stored at -35 °C to obtain off-white needles (with pink edges). The supernatant was decanted carefully and 4 mL fresh ether was added and the vial was stored again at -35 °C. After this time, the needles no longer had any colored attributes. The supernatant was carefully decanted and the off-white needles were crushed and dried under vacuum to yield 42.4 mg of [(CD<sub>3</sub>)<sub>2</sub>Pt<sup>II</sup>(μ-SMe<sub>2</sub>)]<sub>2</sub> in 74% yield. Smaller-scale syntheses were significantly detrimental to yields.

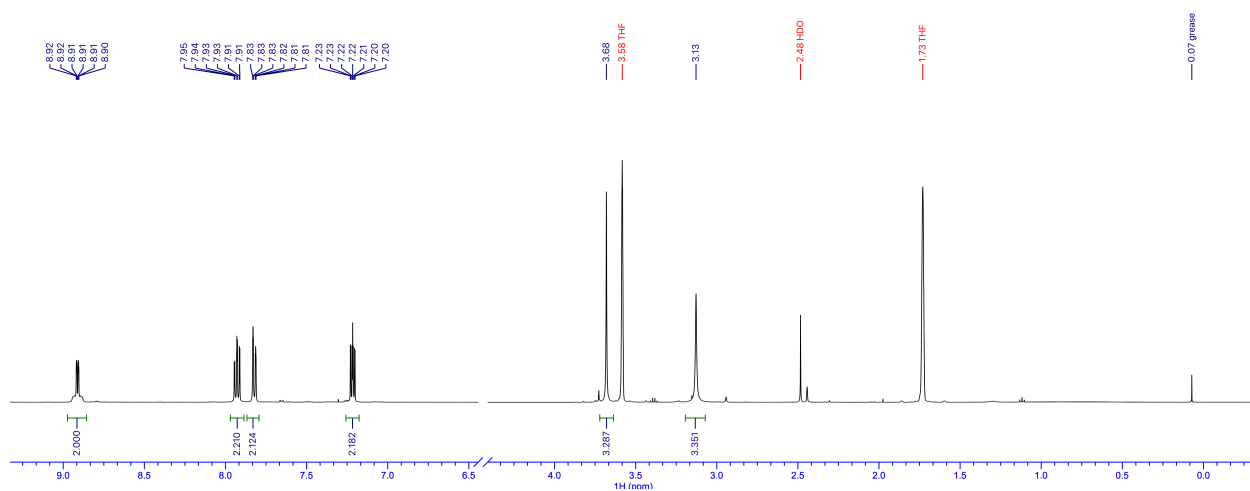
<sup>1</sup>H NMR (25 °C, 400.13 MHz, Acetone-d<sub>6</sub>, ppm) δ: 2.75 (s+Pt-satellites, <sup>3</sup>J<sub>Pt-H</sub> = 21.1 Hz, 12H, SCH<sub>3</sub>)

**Figure S22.** <sup>1</sup>H NMR spectrum of [(CD<sub>3</sub>)<sub>2</sub>Pt<sup>II</sup>(μ-SMe<sub>2</sub>)]<sub>2</sub> in Acetone-d<sub>6</sub>

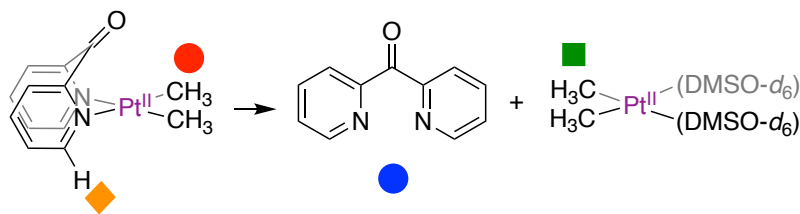


**Synthesis of 2-d<sub>6</sub>:** Complex **2-d<sub>6</sub>** was synthesized using 25 mg of  $[(\text{CD}_3)_2\text{Pt}^{\text{II}}(\mu\text{-SMe}_2)]_2$  (43  $\mu\text{mol}$ ) and 18 mg of 2,2'-(1-methoxyethane-1,1-diyl)dipyridine in a manner identical to that described for the synthesis of **2**. Figure S23 shows the absence of resonances corresponding to the  $\text{Pt}^{\text{II}}\text{-CH}_3$  fragments in  $^1\text{H}$  NMR spectrum.

**Figure S23.**  $^1\text{H}$  NMR spectrum of **2-d<sub>6</sub>** in  $\text{THF-d}_8$  (showing the absence of  $\text{Pt}^{\text{II}}\text{-CH}_3$  resonances)



### S3.4 Reaction of **1** with $\text{DMSO-d}_6$ :



10 mg **1** was charged into a J. Young NMR tube and 0.6 mL  $\text{DMSO-d}_6$  was added. An initially deep-red solution started to bleach in  $\sim 10$  minutes at which point  $^1\text{H}$  NMR analysis (Figure S24) revealed that the major component of the reaction mixture was already free ligand (indicated by blue circles) and  $(\text{DMSO-d}_6)\text{Pt}^{\text{II}}(\text{CH}_3)_2$  ( $\text{Pt-CH}_3$  indicated by green square). Note (Figure S24, Inset): the doublet at 8.77 ppm with corresponding Pt-satellites ( $^3J_{\text{Pt-H}} = 22.5$  Hz, orange diamonds) corresponds to the py-6-CH fragments of **1**; the doublet at 8.68 ppm does not have Pt-satellites. The  $\text{Pt}^{\text{II}}\text{-CH}_3$  resonance of residual complex **1** is indicated by a red circle. In  $\sim 2$  h, the  $^1\text{H}$  NMR spectrum (Figure S25) of the straw-colored corresponded to free DPK and  $(\text{DMSO-d}_6)\text{Pt}^{\text{II}}(\text{CH}_3)_2$ . In a separate experiment, 10 mg of  $[(\text{CH}_3)_2\text{Pt}^{\text{II}}(\mu\text{-SMe}_2)]_2$  was dissolved in  $\text{DMSO-d}_6$  and was analyzed by  $^1\text{H}$  NMR spectroscopy  $\sim 2$  hours after dissolution (Figure S26). The resonance corresponding to the  $\text{Pt-CH}_3$  fragment (0.50 ppm,  $^2J_{\text{Pt-H}} = 79.5$  Hz) shown in Figure S26 is an exact match to that in Figure S25. Free  $\text{SMe}_2$  appears as a singlet (without Pt-satellites) at 2.05 ppm.

Figure S24. <sup>1</sup>H NMR spectrum of **1** in DMSO-*d*<sub>6</sub>, ~10 min after dissolution:

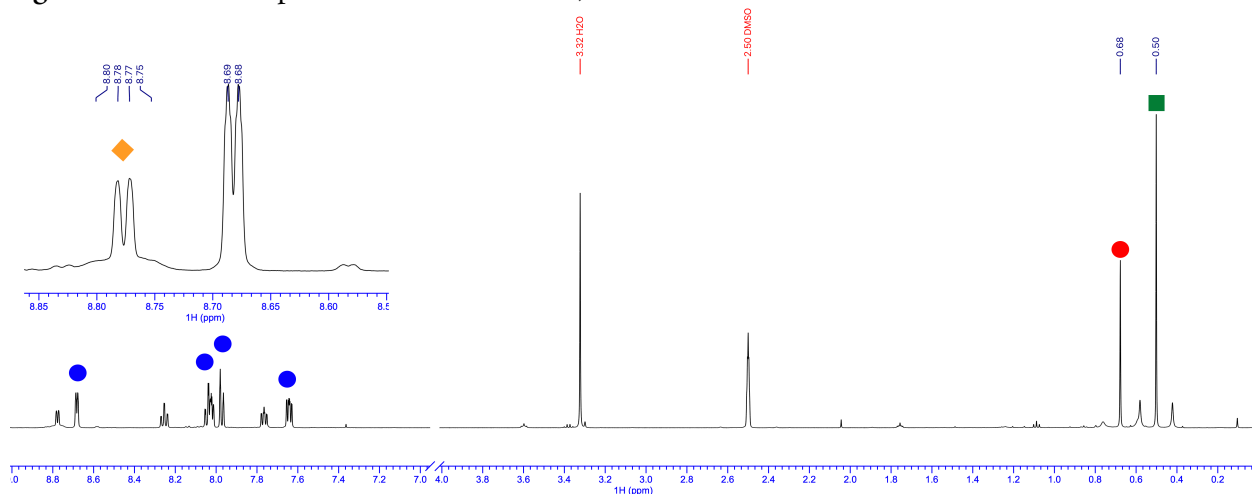


Figure S25. <sup>1</sup>H NMR spectrum of **1** in DMSO-*d*<sub>6</sub>, ~2 h after dissolution:

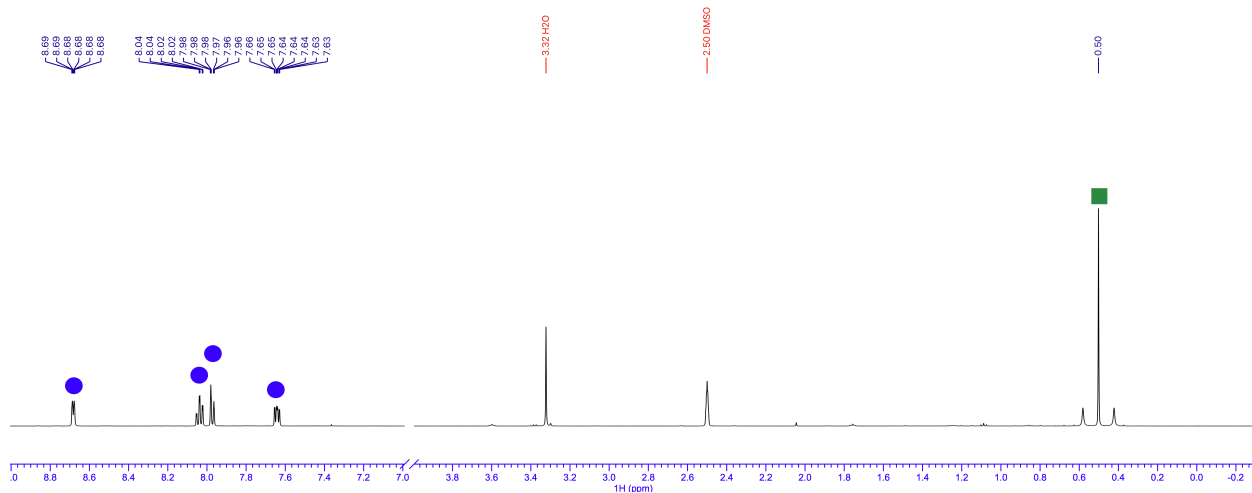
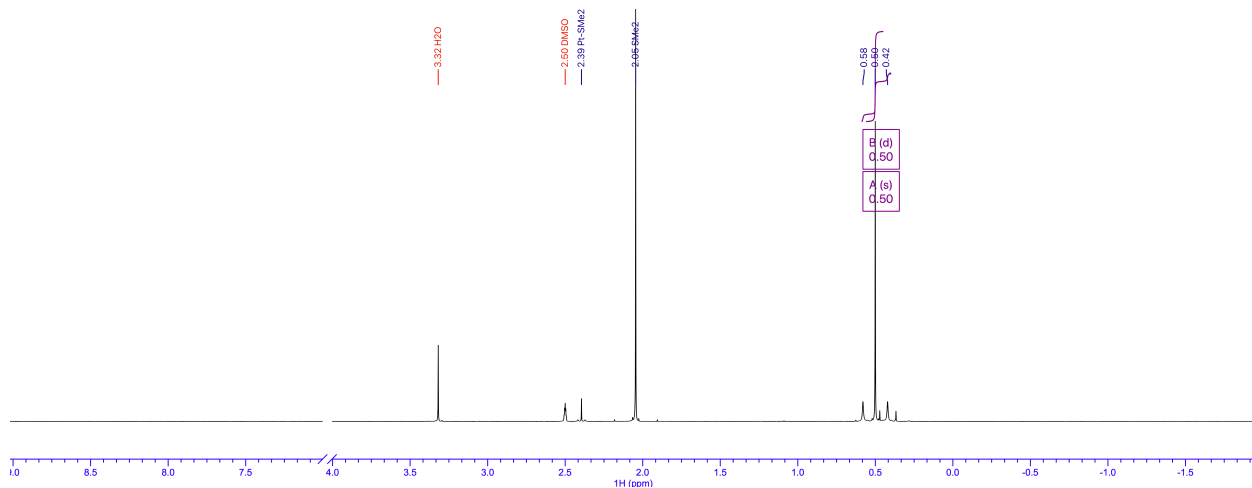


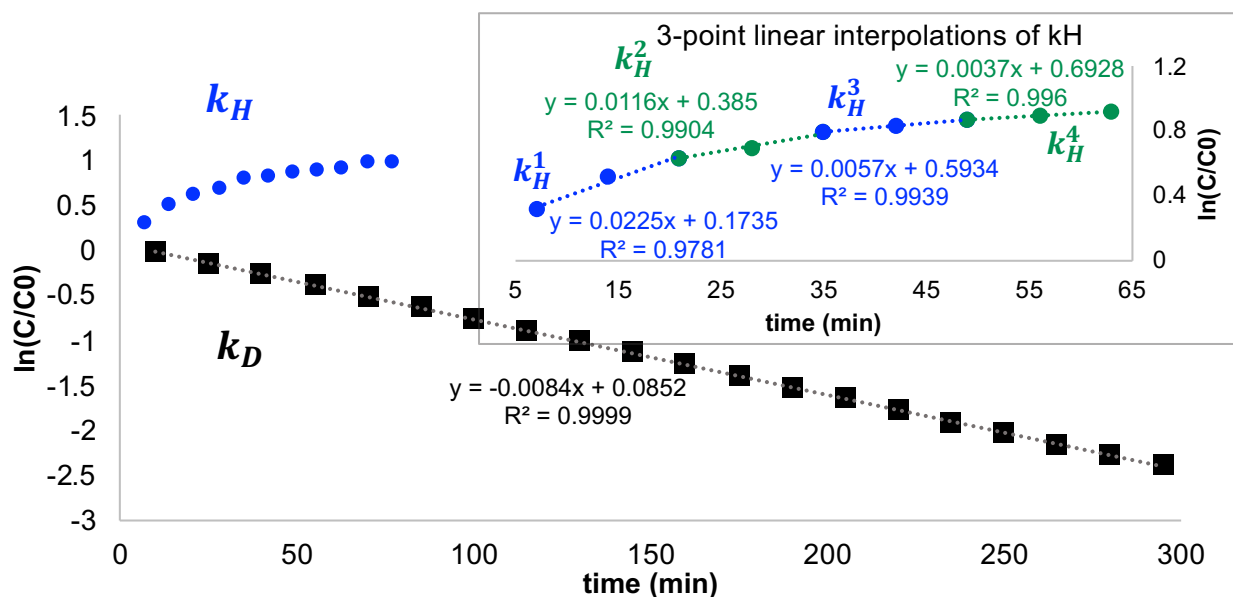
Figure S26. <sup>1</sup>H NMR spectrum of  $[(CH_3)_2Pt^{II}(DMSO-d_6)]_2$  in DMSO-*d*<sub>6</sub>:



### S3.5 Determination of KIEs for complexes **1**/**1-d<sub>6</sub>** and **2**/**2-d<sub>6</sub>**:

**Protonation of **1-d<sub>6</sub>**:** 3 mg of **1-d<sub>6</sub>** was dissolved in 0.25 mL CD<sub>3</sub>OH in a capillary and quickly transferred to a J. Young NMR tube and inserted into the NMR spectrometer that had been pre-shimmed and pre-tuned to CD<sub>3</sub>OD. The reaction of **1-d<sub>6</sub>** with CD<sub>3</sub>OH was monitored by <sup>1</sup>H NMR spectroscopy at 7-minute intervals. Figure S27 shows the comparison of the rate of protonation ( $k_H$ ) to the rate of deuteration ( $k_D$ ). As opposed to the deuteration reaction which maintains a constant rate of  $8.4 \times 10^{-3} \text{ min}^{-1}$ , the rate of protonation was found to decrease over time. From rates of protonation ( $k_H$ ) obtained from 3-point linear interpolations, the ratio of isotope effect was calculated to be  $k_H/k_D = 2.6$  in initial rate conditions (7-21 min), further decreasing to  $k_H^2/k_D = 1.4$  (21-35 min) and  $k_H^3/k_D = 0.6$  (35-49 min). This is simply due to the thumb-rule that “deuterium prefers to reside in the site corresponding to the higher frequency oscillator”<sup>6</sup>. Since the stretching frequencies of PtC-H and MeO-H fragments are  $\sim 2900 \text{ cm}^{-1}$  and  $\sim 3500 \text{ cm}^{-1}$ , respectively, the isodesmic reactions **1-d<sub>n</sub>** + CD<sub>3</sub>OD  $\rightarrow$  **1-d<sub>(n+1)</sub>** + CD<sub>3</sub>OH are endergonic (see Table S2 and related discussion in the Computational Section). This implies that at any step, the reactants for the deuteration reaction are at a lower energy (therefore, higher barrier for reductive coupling) than the reactants for the protonation reaction. Qualitatively speaking, as the protonation reaction proceeds, the ‘new’ starting materials are at a lower energy, making subsequent barriers higher, and thus the reaction slower and slower. A full computational analysis of all isotopomers involved (**1-d<sub>n</sub>**;  $n = 0-6$ ), including symmetrically and asymmetrically deuterated complexes, as well as secondary kinetic effects, while interesting, is beyond the scope of the current work.

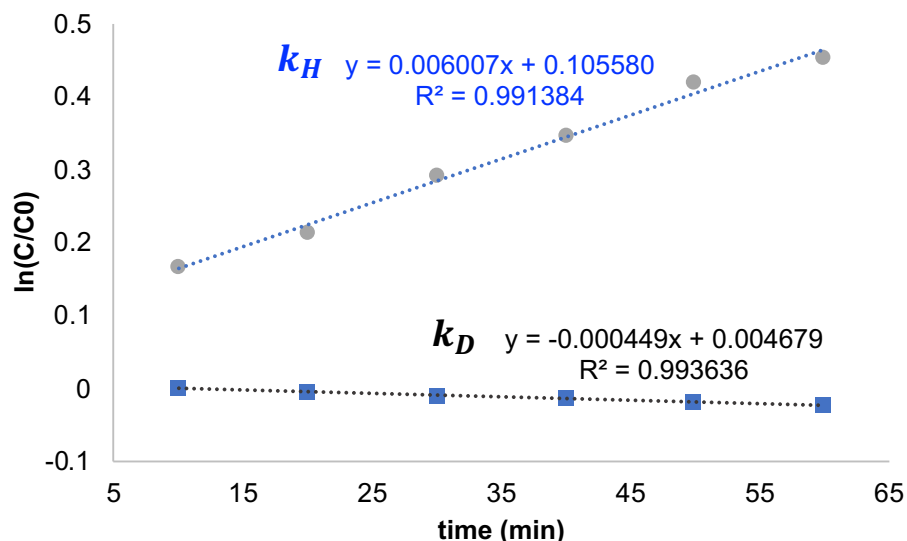
**Figure S27.** Comparison of rates<sup>†</sup> of reaction of **1** with CD<sub>3</sub>OD ( $k_D$ , black squares) to that of **1-d<sub>6</sub>** with CD<sub>3</sub>OH ( $k_H$ , blue circles) with 3-point linear interpolations for  $k_H$



<sup>†</sup> C and C<sub>0</sub> are the total integral intensities of Pt-CH<sub>x</sub>D<sub>3-x</sub> fragments observed in the <sup>1</sup>H NMR spectra at t and t=0 respectively

**Protonation of **2-d<sub>6</sub>**:** 2 mg **2-d<sub>6</sub>** was dissolved in 0.25 mL CD<sub>3</sub>OH in a capillary and quickly transferred to a J. Young NMR tube and inserted into the NMR spectrometer that has been pre-shimmed and pre-tuned to CD<sub>3</sub>OD. The reaction of **2-d<sub>6</sub>** with CD<sub>3</sub>OH was monitored at 10 minutes intervals. Figure S28 shows the comparison of the initial rate of protonation ( $k_H$ ; 10-60 mins) to the rate of deuteration ( $k_D$ ; 10-60 mins). Based on initial rates, a  $k_H/k_D = 13.1$  was calculated.

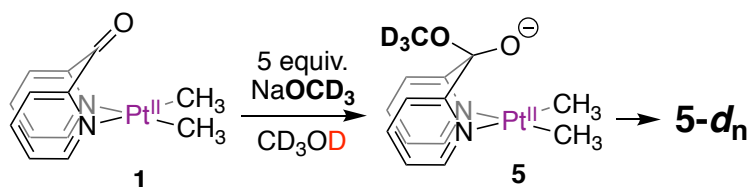
**Figure S28.** Comparison of rates<sup>†</sup> of reaction of **2** with CD<sub>3</sub>OD ( $k_D$ , black) to that of **2-d<sub>6</sub>** with CD<sub>3</sub>OH ( $k_H$ , blue)



<sup>†</sup>C and C<sub>0</sub> are the total integral intensities of Pt-CH<sub>x</sub>D<sub>3-x</sub> fragments observed in the <sup>1</sup>H NMR spectra at t and t=0 respectively

### S3.6 Support for the electrophilic involvement of the keto fragment of DPK:

#### 3.6.1 In situ observation of **5** and concomitant Pt<sup>II</sup>-CH<sub>3</sub> deuteration: 3 mg (125 μmol) NaH was weighed



out into a vial and chilled in the freezer of the glove-box. To this vial was carefully added chilled (-35 °C) 0.6 mL CD<sub>3</sub>OD. In a separate vial, 10 mg (24 μmol) complex **1** was weighed and the NaOCD<sub>3</sub> solution was carefully added.

Unlike neutral solutions of **1** in methanol which are orange-red, the alkaline solution of the complex assumed a pale peach-like color. The solution was transferred to a J. Young NMR tube and analyzed by <sup>1</sup>H and <sup>13</sup>C NMR spectroscopy. At room temperature, the <sup>1</sup>H NMR spectrum of **5** indicates fluxional character of the complex, presumed to be because of rapid interconversion of isomers with *exo* and *endo* OCD<sub>3</sub> fragments, consistent with broadened <sup>1</sup>H resonances (*vide infra*). At -15 °C, the resonances sharpened and <sup>13</sup>C NMR spectra indicated the absence of keto fragment (ca. 188 ppm) and the presence of a signal at 104.9 ppm (corresponding to the py<sub>2</sub>C) fragment of the 'hemiketalate' complex, **5**. Deuteration ( $k_D = 0.0021 \text{ min}^{-1}$ ) of the Pt<sup>II</sup>-CH<sub>3</sub> fragment was observed at a rate much slower than that observed for the deuteration of **1** under neutral conditions ( $k_D = 0.0084 \text{ min}^{-1}$ ). Attempts to observe the anionic **5** by ESI(-)-MS were unsuccessful.

**<sup>1</sup>H NMR** (-15 °C, 400.13 MHz, CD<sub>3</sub>OD, ppm)  $\delta$ : 8.79 (d+Pt-shoulders,  $J_{H-H} = 5.34 \text{ Hz}$ , 2H, py-6-CH), 8.24 (d,  $J_{H-H} = 7.86$ , 2H, py-CH), 7.98 (td,  $J_{H-H} = 7.7$ , 1.3 Hz, 2H, py-CH), 7.29 (td, 7.1, 5.8, 1.4 Hz, 2H, py-CH), 0.72 (s+Pt-satellites,  $^2J_{Pt-H} = 74.3 \text{ Hz}$ , ~6H, Pt<sup>II</sup>-CH<sub>3</sub>)

**<sup>13</sup>C NMR** (-15 °C, 125.78 MHz, CD<sub>3</sub>OD, ppm)  $\delta$ : 163.6, 150.8, 137.3, 125.4, 125.1, 104.9 (py<sub>2</sub>C), -19.0 (s+Pt-satellites,  $^1J_{Pt-C} \sim 810 \text{ Hz}$ ). An additional set of signals corresponding to a minor unidentified species were also observed (indicated by \* in the <sup>13</sup>C NMR spectrum): 151.3, 139.4, 129.7, 126.6, -15.79

**Figure S29.**  $^1\text{H}$  NMR spectrum of **5** ( $-15\text{ }^\circ\text{C}$ ) in  $\text{CD}_3\text{OD}$  (prepared as described above)

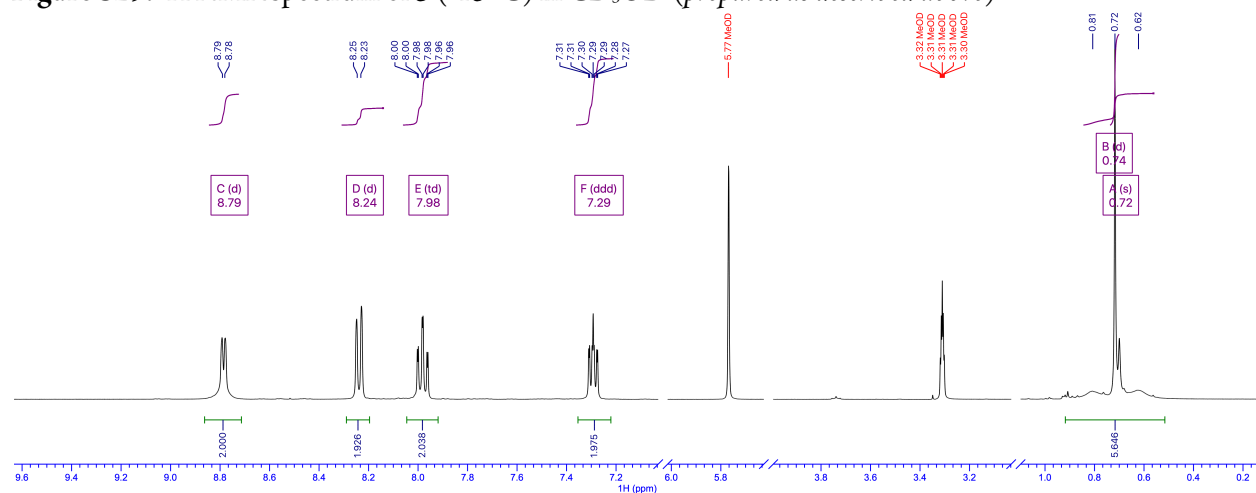


**Figure S30.**  $^{13}\text{C}$  NMR spectrum of **5** ( $-15\text{ }^\circ\text{C}$ ) in  $\text{CD}_3\text{OD}$  (prepared as described above)

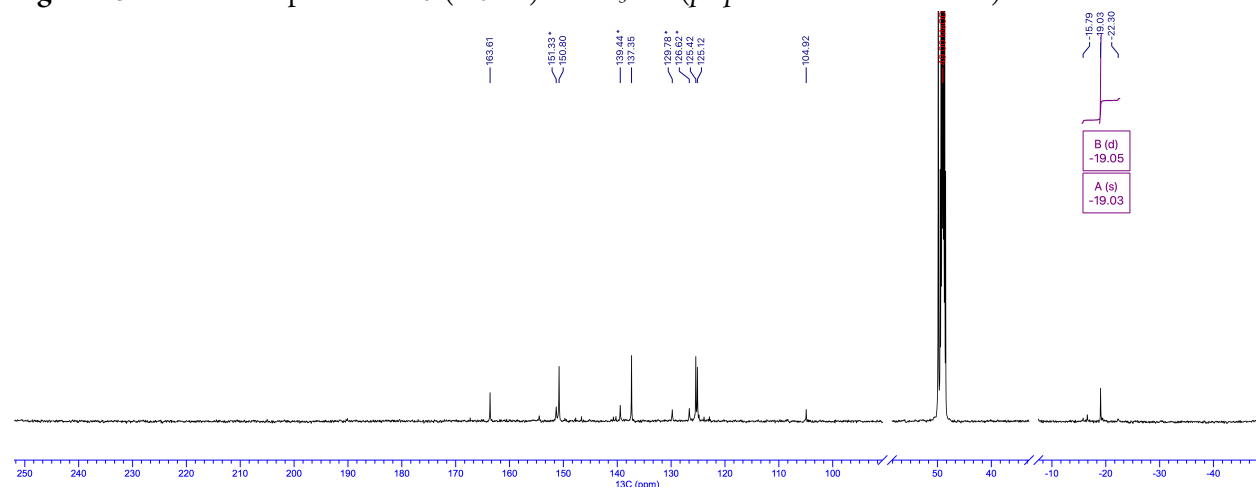


**Figure S31.** Stacked  $^1\text{H}$  NMR plot showing deuteration of  $\text{Pt}^{\text{II}}\text{-CH}_3$  fragments of **5**

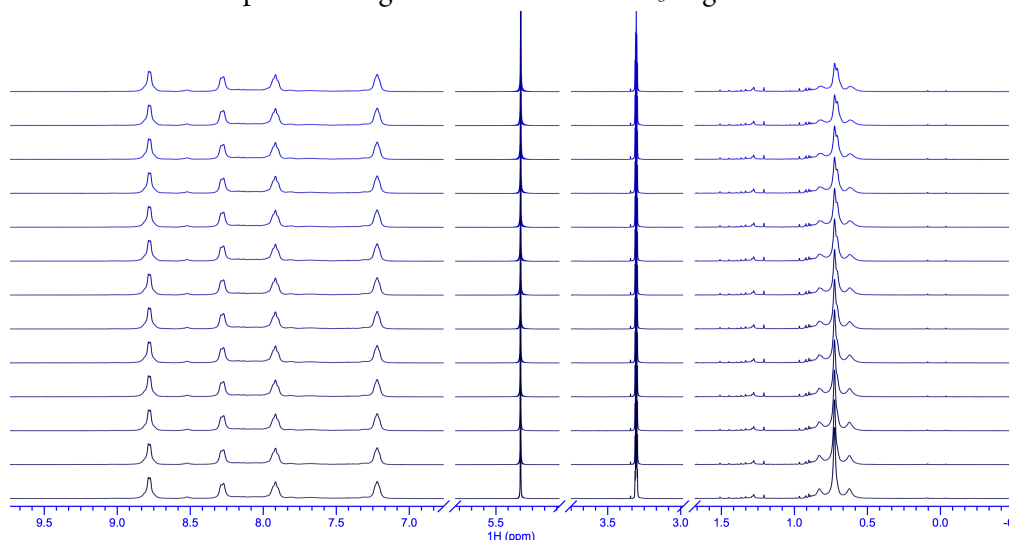
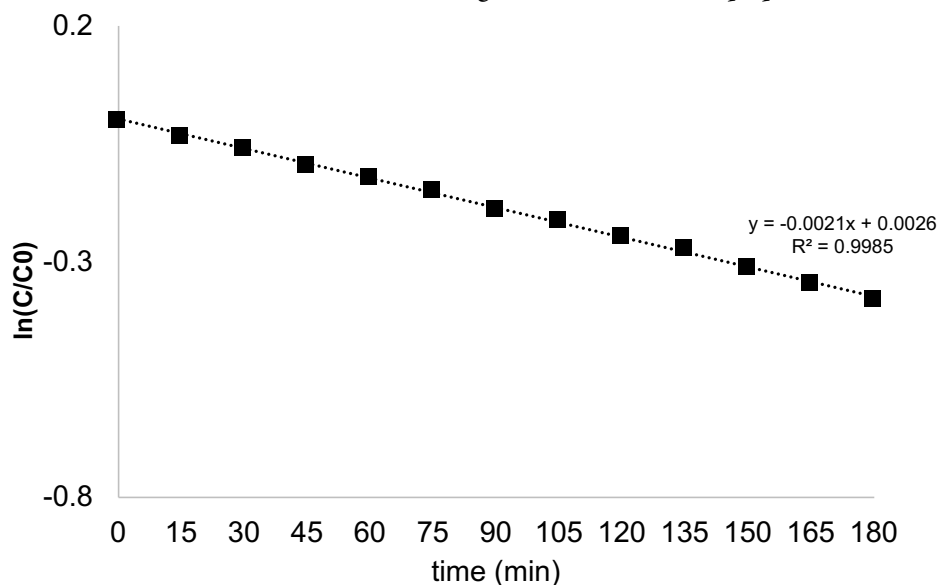
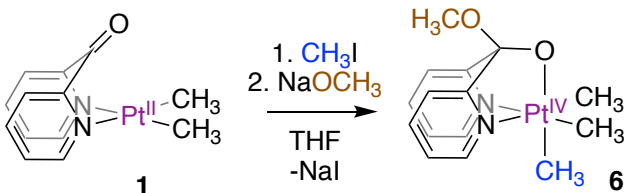


**Figure S32.** Rate<sup>+</sup> of deuteration of the Pt<sup>II</sup>-CH<sub>3</sub> fragments of **5** at 25 °C (prepared as described above)



<sup>+</sup>C and C<sub>0</sub> are the total integral intensities of Pt-CH<sub>x</sub>D<sub>3-x</sub> isotopologues observed in the <sup>1</sup>H NMR spectra at t and t=0 respectively

**S3.6.2 Synthesis of 6:** A Schlenk-tube was charged with 30 mg (73 μmol) of **1** and a stir-bar inside the glove box. To this ~8 mL THF was added to obtain a wine-red solution of **1**. The tube was capped with a rubber septum and taken out of the glove-box, and 5 μL (1.1 equiv.) methyl iodide was added via gas-tight syringe through the septum at room temperature with stirring. Immediately, the wine-red color bleached to form a pale-yellow suspension. After 10 minutes, 15 μL of a 5 M solution of sodium methoxide in methanol was added. Immediately, a colorless supernatant and fine white precipitate was observed. The contents of the Schlenk-tube were dried under vacuum and taken into the glove-box. The solids



were re-dispersed in 5 mL THF and filtered through a 0.4 μm PTFE syringe filter and the contents were evacuated to obtain 30.5 mg of **6** as a white analytically pure powder in 91% yield.

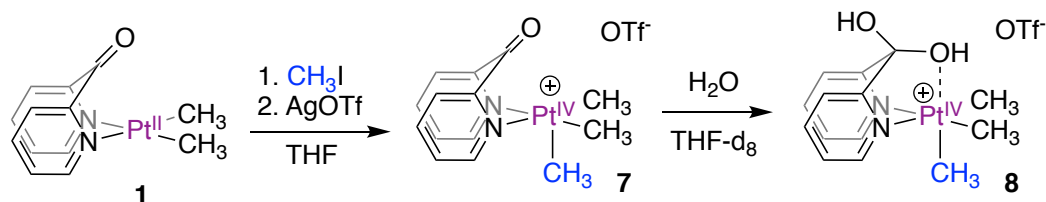
<sup>1</sup>H NMR (25 °C, 400.2 MHz, C<sub>6</sub>D<sub>6</sub>, ppm) δ: 8.06 (d+Pt-satellites, J<sub>H-H</sub> = 5.5. Hz, <sup>3</sup>J<sub>Pt-H</sub> = 12.6 Hz, 2H, py-6-CH), 7.51 (d, J<sub>H-H</sub> = 7.8 Hz, 2H, py-3-CH), 6.87 (td, J<sub>H-H</sub> = 7.6, 1.4 Hz, 2H, py-5-CH), 6.28 (m, 2H, py-4-CH), 3.72 (s, 3H, OCH<sub>3</sub>), 1.59 (s+Pt-satellites, <sup>2</sup>J<sub>Pt-H</sub> = 73.4 Hz, 6H, equatorial Pt<sup>IV</sup>-CH<sub>3</sub>), 1.25 (s+Pt-satellites, <sup>2</sup>J<sub>Pt-H</sub> = 70.5 Hz, 3H, axial Pt<sup>IV</sup>-CH<sub>3</sub>)

<sup>13</sup>C NMR (25 °C, 400.2 MHz, C<sub>6</sub>D<sub>6</sub>, ppm) δ: 164.96 (s+Pt-satellites, J<sub>Pt-C</sub> = 11 Hz, py), 145.21 (s+Pt-satellites, J<sub>Pt-C</sub> = 14.2 Hz, py), 137.47 (s+Pt-shoulders, J<sub>Pt-C</sub> ~ 4 Hz), 123.37 (s+Pt-satellites, J<sub>Pt-C</sub> = 13.4 Hz), 121.21 (s+Pt-satellites, J<sub>Pt-C</sub> = 7.7 Hz), 110.08 (s, py<sub>2</sub>C), 49.54 (s, OCH<sub>3</sub>), -10.97 (s+Pt-satellites, <sup>1</sup>J<sub>Pt-C</sub> = 702.5 Hz, equatorial Pt<sup>IV</sup>-CH<sub>3</sub>), -13.74 (s+Pt-satellites, <sup>1</sup>J<sub>Pt-C</sub> = 688.8 Hz, axial Pt<sup>IV</sup>-CH<sub>3</sub>)

**Elemental Analysis: (C, H, N):** Calculated: 39.56, 4.43, 6.15; Found: 39.20, 4.71, 6.20



### S3.6.3. Synthesis of complex **7** and **8**:



A Schlenk-tube was charged with 30 mg (73  $\mu\text{mol}$ ) of **1** and a stir-bar inside the glove box. To this  $\sim 8$  mL THF was added to obtain a wine-red solution of **1**. The tube was capped with a rubber septum and taken out of the glove-box, and 5  $\mu\text{L}$  (1.1 equiv.) methyl iodide was added via gas-tight syringe through the septum at room temperature with stirring. Immediately, the wine-red color bleached to form a pale-yellow suspension. The contents of the Schlenk-tube were dried under vacuum and taken into the glove-box. In a vial, 19 mg (1 equiv.) AgOTf was dissolved in 2 mL THF and the solution added to the solids in the Schlenk-tube with vigorous stirring. An additional 2 mL (1 mL x 2 times) was used to complete the transfer. Immediately a fine white precipitate (AgCl) and colorless supernatant were obtained. The contents were filtered through a 0.4  $\mu\text{m}$  PTFE syringe filter and the obtained filtrate was dried under vacuum to obtain 38.5 mg of **7** as a fine white powder in 89% yield. Satisfactory Elemental Analysis could not be obtained owing to the hygroscopic nature of the complex. <sup>1</sup>H and <sup>13</sup>C NMR spectra and High-resolution ESI-MS analysis are being provided to demonstrate sample homogeneity. For the observation of **8**, 15  $\mu\text{L}$  water was added to a 0.6 mL THF-*d*<sub>8</sub> solution containing 18 mg of **7**. Single crystals suitable for X-ray diffraction were obtained upon slow evaporation of the THF-solution of **8**.

<sup>1</sup>H NMR (25 °C, 500.15 MHz, CD<sub>3</sub>CN, ppm)  $\delta$ : 8.82 (d+Pt-satellites,  $J_{\text{H-H}} = 5.8$  Hz,  $^3J_{\text{Pt-H}} = 15.7$  Hz, 2H, py-6-CH), 8.31 (td,  $J_{\text{H-H}} = 8.0, 1.4$  Hz, 2H, py-CH), 8.19 (vd,  $J_{\text{H-H}} = 7.9$  Hz, 2H, py-CH), 7.89 (ddd,  $J_{\text{H-H}} = 7.5, 5.4, 1.3$  Hz, 2H, py-CH), 1.12 (s+Pt-satellites,  $^2J_{\text{Pt-H}} = 69$  Hz, 6H, equatorial Pt<sup>IV</sup>-CH<sub>3</sub>), 0.93 (s+Pt-satellites,  $^2J_{\text{Pt-H}} = 75.3$  Hz, 3H, axial Pt<sup>IV</sup>-CH<sub>3</sub>)

<sup>13</sup>C NMR (25 °C, 125.78 MHz, CD<sub>3</sub>CN, ppm)  $\delta$ : 190.6 (s+Pt-satellites,  $J_{\text{Pt-C}} = 17.1$  Hz, C=O), 152.4 (s+Pt-satellites,  $J_{\text{Pt-C}} = 4.8$  Hz, py), 150.47 (s+Pt-satellites,  $J_{\text{Pt-C}} = 7.0$  Hz, py), 142.18 (py), 131.02 (s+Pt-satellites,  $J_{\text{Pt-C}} = 14.0$  Hz, py), 128.57 (s+Pt-satellites,  $J_{\text{Pt-C}} = 5.9$  Hz, py), -3.60 (s+Pt-satellites,  $^2J_{\text{Pt-C}} = 739.3$  Hz, axial Pt<sup>IV</sup>-CH<sub>3</sub>), -5.79 (s+Pt-satellites,  $^2J_{\text{Pt-C}} = 673.6$  Hz, equatorial Pt<sup>IV</sup>-CH<sub>3</sub>)

**High-Resolution ESI<sup>+</sup>-MS:** Complex **7**: Calculated for C<sub>14</sub>H<sub>17</sub>N<sub>2</sub>OPt: 423.0962; Found: 423.0964.

**Figure S36.** <sup>1</sup>H NMR spectrum of **7** in CD<sub>3</sub>CN

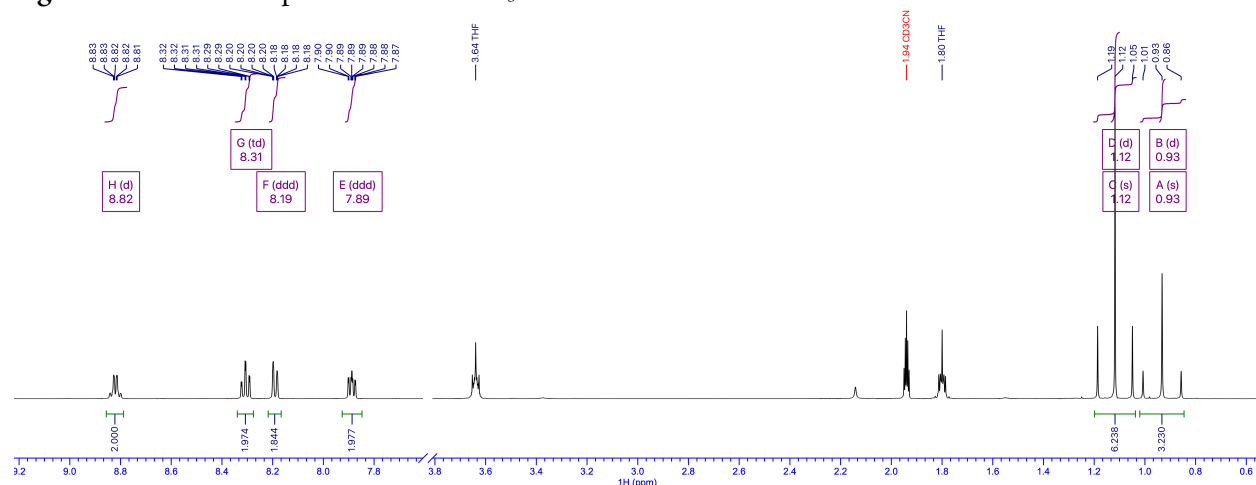
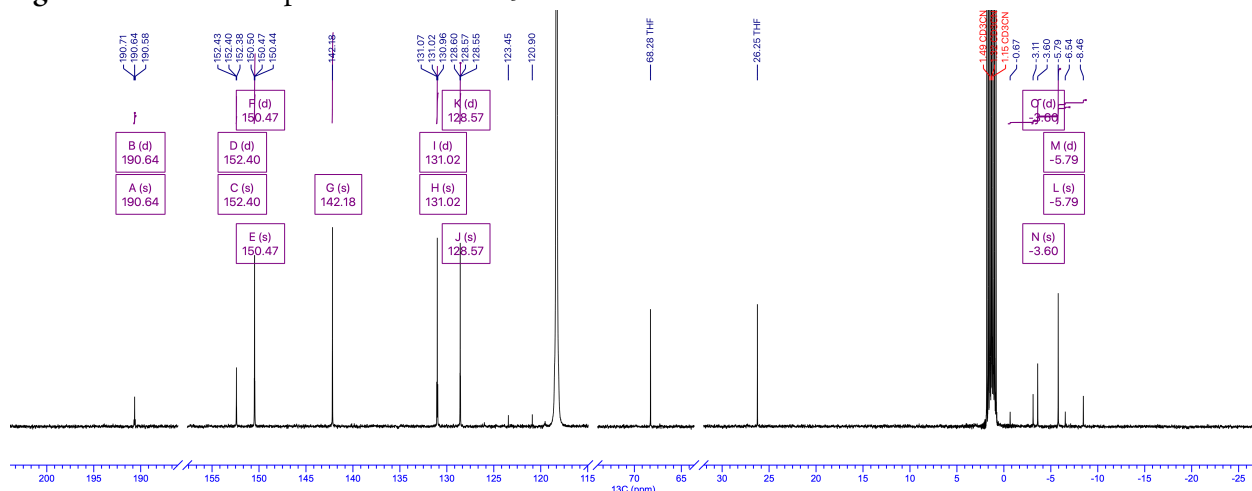


**Figure S37.**  $^{13}\text{C}$  NMR spectrum of **7** in  $\text{CD}_3\text{CN}$



Complex **8**, recorded after addition of  $\text{H}_2\text{O}$  to a  $\text{THF-}d_8$  solution of complex **7**:

$^1\text{H}$  NMR (25 °C, 500.15 MHz,  $\text{THF-}d_8$ , ppm)  $\delta$ : 8.61 (d+Pt-shoulders,  $J_{\text{H-H}} = 4.7$  Hz, 2H, py-6-CH), 8.21 (td,  $J_{\text{H-H}} = 7.7$  Hz, 2H, py-CH), 8.06 (d,  $J_{\text{H-H}} = 7.8$  Hz, 2H, py-CH), 7.69 (t,  $J_{\text{H-H}} = 5.6$  Hz, 2H, py-CH), 1.32 (s+Pt-satellites,  $^3J_{\text{Pt-H}} = 80.8$  Hz, 3H, axial  $\text{Pt}^{\text{IV}}\text{-CH}_3$ ), 0.97 (s+Pt-satellites,  $^3J_{\text{Pt-H}} = 70.8$  Hz, 6H, equatorial  $\text{Pt}^{\text{IV}}\text{-CH}_3$ )

$^{13}\text{C}$  NMR (25 °C, 125.78 MHz,  $\text{THF-}d_8$ , ppm)  $\delta$ : 157.70 (py), 147.01 (py), 142.03 (py), 127.70 (s+Pt-shoulders, py), 123.82 (py), 103.12 ( $\text{py}_2\text{C}(\text{OH})_2$ ), -9.64 (s+Pt-satellites,  $^1J_{\text{Pt-C}} = 760.4$  Hz,  $\text{Pt}^{\text{IV}}\text{-CH}_3$ ), -9.94 (s+Pt-satellites,  $^1J_{\text{Pt-C}} = 676.3$  Hz,  $\text{Pt}^{\text{IV}}\text{-CH}_3$ )

**High-Resolution ESI<sup>+</sup>-MS** [Recorded in methanol, spectrum corresponds to methanol adduct of **7**]  
 Calculated for  $\text{C}_{15}\text{H}_{21}\text{N}_2\text{O}_2\text{Pt}$ : 456.1251, Found: 456.1246

**Figure S38.**  $^1\text{H}$  NMR spectrum of **8** in  $\text{THF-}d_8$

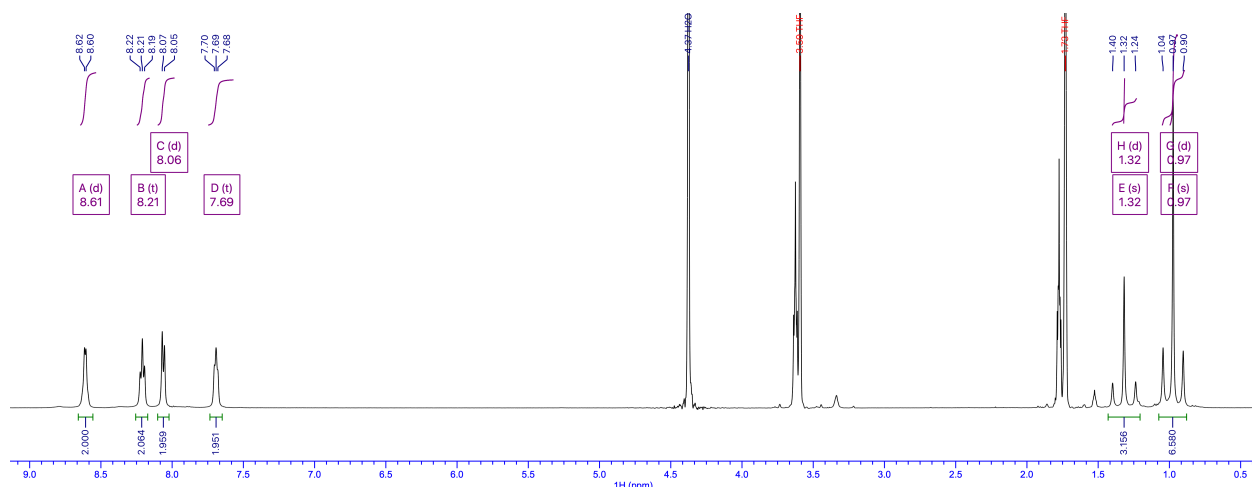
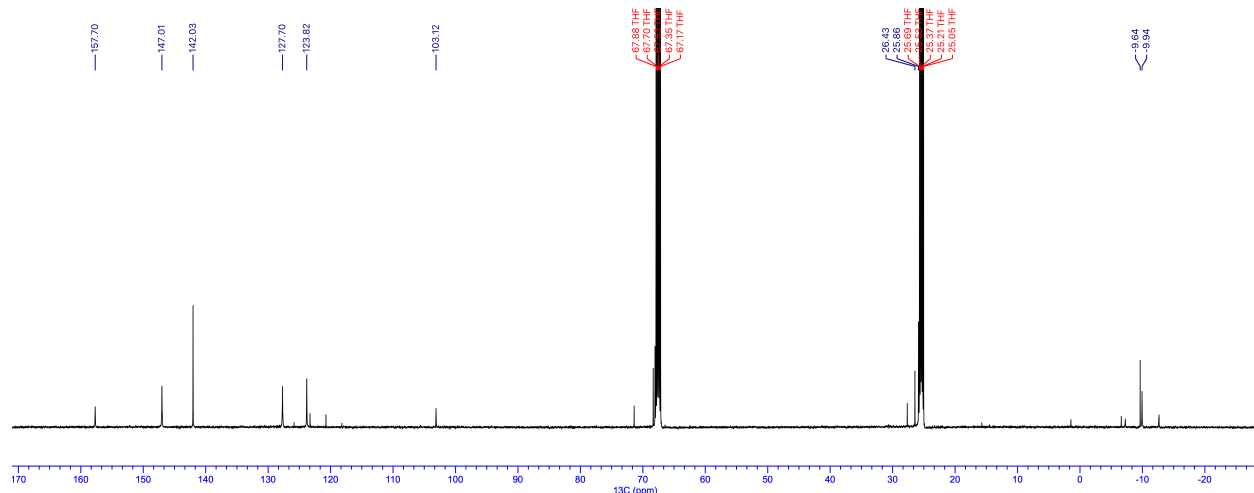


**Figure S39.**  $^{13}\text{C}$  NMR spectrum of **8** in  $\text{THF-}d_8$



#### S3.6.4. Attempted reaction of complexes **1** and **2** with AcOD in $\text{THF-}d_8$ :

10 mg (24  $\mu\text{mol}$ ) **1** was dissolved in 0.5 mL  $\text{THF-}d_8$  and the wine-red solution was transferred to a screw-cap NMR tube equipped with a septum and the NMR tube was sealed taken out of the glove-box. The solution was chilled to 0  $^\circ\text{C}$  using an ice-bath and 70  $\mu\text{L}$  (~50 equiv.) AcOD was injected through the septum. The tube was shaken and monitored by  $^1\text{H}$  NMR spectroscopy (every one hour for 12 h, see Figure S40). The reaction of complex **2** was similarly attempted using 10 mg of **2** (22  $\mu\text{mol}$ ) and 70  $\mu\text{L}$  (~50 equiv.) AcOD and monitored by  $^1\text{H}$  NMR spectroscopy (see Figure S41). In both cases, while deuteration of the Pt- $\text{CH}_3$  fragments was observed, no methane loss was observed in the course of 12 h.

**Figure S40.** Stacked plot of the  $^1\text{H}$  NMR spectra of the reaction of **1** with AcOD in  $\text{THF-}d_8$ :

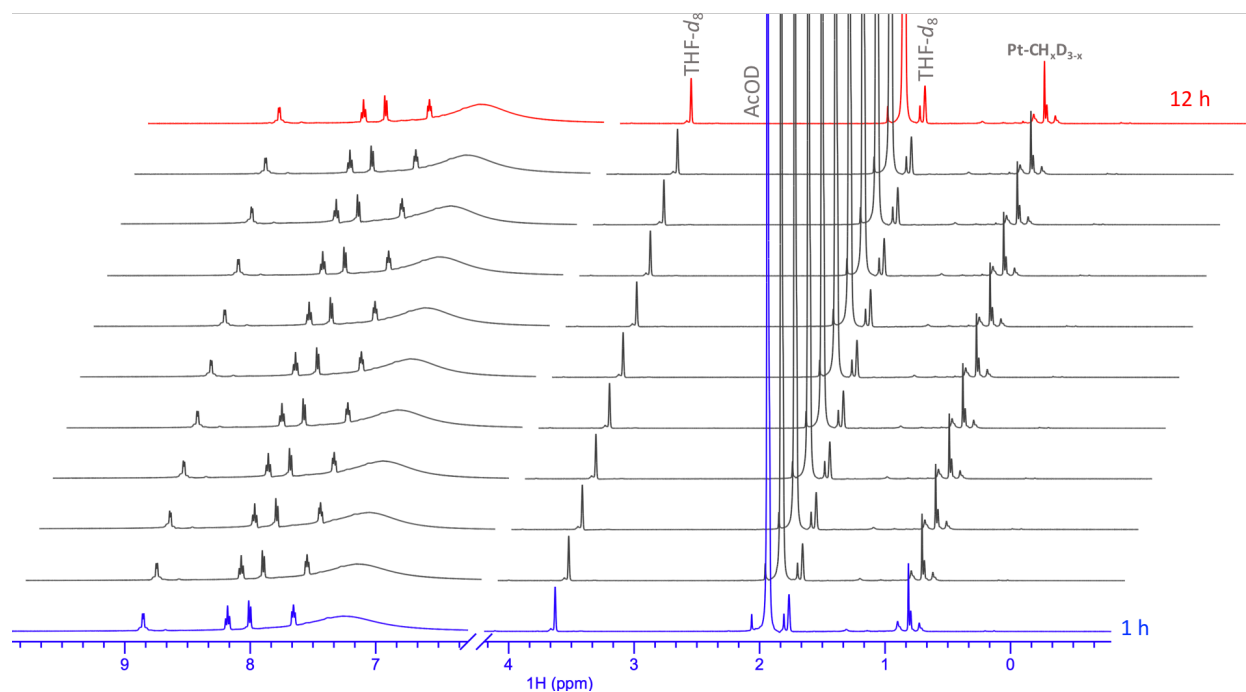
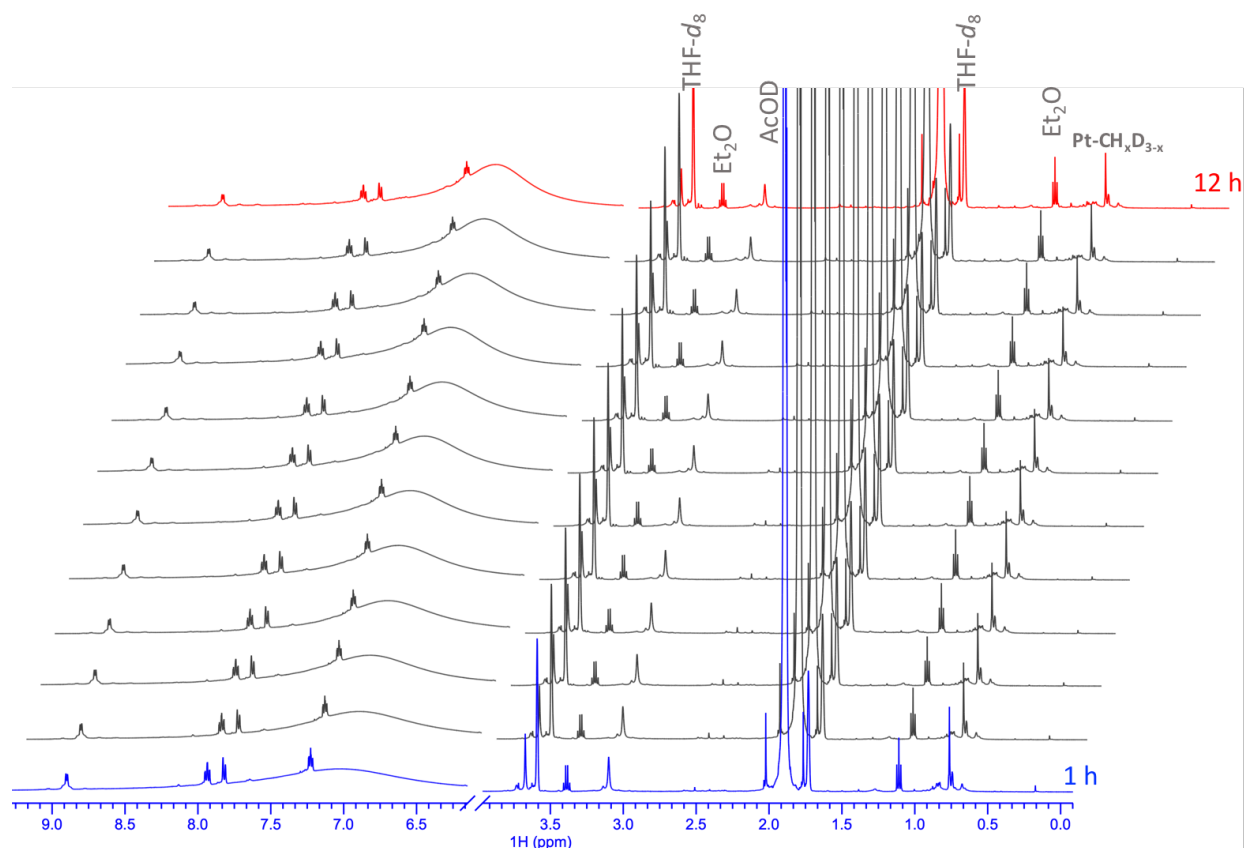


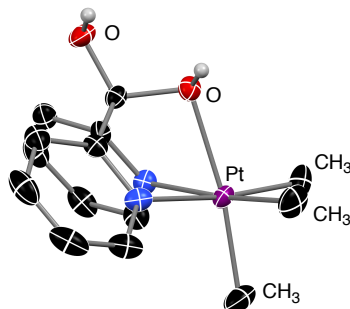
**Figure S41.** Stacked plot of the  $^1\text{H}$  NMR spectra of the reaction of **2** with AcOD in  $\text{THF-d}_8$ :



-----End of Section 3-----

## S4. Details of X-ray crystallographic characterization of complex 8

---



The crystal of complex **8** was mounted on a CryoLoop (Hampton Research Corp.) with a layer of light mineral oil and placed in a nitrogen stream at 123(2) K. Measurements were made on a Rigaku Varimax with HyPix diffractometer using mirror-monochromated Mo-K $\alpha$  radiation. The structure was solved by direct methods (SHELXT<sup>7</sup>). The structure was refined on  $F^2$  by the full-matrix least-squares method using SHELXL<sup>8</sup> using Olex2 program.<sup>9</sup> The non-hydrogen atoms were anisotropically refined, while the hydrogen atoms were refined using the riding model. The molecular structure was disordered with a 0.947(4):0.053(4) ratio.

### Crystal Data and Data Collection Parameters

---

CCDC	2027312
Empirical formula	C <sub>15</sub> H <sub>19</sub> F <sub>3</sub> N <sub>2</sub> O <sub>5</sub> PtS
Formula weight	591.47
Temperature/K	123
Crystal system	monoclinic
Space group	$P2_1/n$
$a/\text{\AA}$	11.3867(2)
$b/\text{\AA}$	13.3132(3)
$c/\text{\AA}$	12.4183(2)
$\alpha/^\circ$	90
$\beta/^\circ$	92.717(2)
$\gamma/^\circ$	90
Volume/ $\text{\AA}^3$	1880.42(6)
$Z$	4
$\rho_{\text{calc}}/\text{g/cm}^3$	2.089
$\mu/\text{mm}^{-1}$	7.631
F(000)	1136.0
Crystal size/ $\text{mm}^3$	0.4 × 0.2 × 0.1
Radiation	Mo-K $\alpha$ ( $\lambda = 0.71073$ )
2 $\theta$ range for data collection/ $^\circ$	4.488 to 58.52
Index ranges	-14 ≤ $h$ ≤ 15, -17 ≤ $k$ ≤ 16, -16 ≤ $l$ ≤ 16
Reflections collected	30286
Independent reflections	4591 [ $R_{\text{int}} = 0.0438$ , $R_{\text{sigma}} = 0.0274$ ]
Data/restraints/parameter	4591/0/262
Goodness-of-fit on $F^2$	1.195
Final R indexes [ $I \geq 2\sigma(I)$ ]	$R_1 = 0.0259$ , $wR_2 = 0.0528$
Final R indexes [all data]	$R_1 = 0.0299$ , $wR_2 = 0.0536$
Largest diff. peak/hole / $e \text{\AA}^{-3}$	0.87/-1.28

---

----- End of Section 4 -----

## S5. Computational Details

DFT calculations were performed using the M06 functional<sup>10</sup> and def2-tzvp basis<sup>11</sup> set for all elements (default ECPs for Pt) as implemented in the Gaussian 16 package.<sup>12</sup> Visualization and vibrational analysis were performed by using the GaussView 6 Package.<sup>13</sup> All structures were fully optimized in solvent (CH<sub>3</sub>OH) using the SMD model.<sup>14</sup> Free energies of ‘deuterated’ structures were calculated by performing frequency calculations on appropriately ‘deuterated’ (by specifying iso=2) structures in solvent. Since neat methanol serves as both as solvent and reactant, the free energy was corrected to account for the change in standard state<sup>15</sup> (24.6 M for CD<sub>3</sub>OD and 24.7 M for CD<sub>3</sub>OH). No corrections were applied for other solutes. The free energy of methoxide-*d*<sub>3</sub> in solution was calculated by adding the free energy of solvation of the methoxide ion ( $\Delta G_{\text{solvation}} = -107.6$  kcal/mol)<sup>16</sup> to the free energy of methoxide-*d*<sub>3</sub> calculated by DFT in the gas-phase (see Table S1). Connectivity between the transition states and corresponding intermediates on either side were established by means of intrinsic reaction coordinate (IRC) calculations at the same level of theory. Analytical frequency calculations (at 298.15 K and 1 atm.) performed on the resultant geometries conformed to exactly ZERO imaginary frequencies for all ground states and exactly ONE imaginary frequency for the transition states. Gibbs free energies are reported as the sum of solvent-corrected electronic and thermal free energies. All geometries are provided as MOL2 files which can be directly opened in any molecule editor, such as Mercury (<https://www.ccdc.cam.ac.uk>), Avogadro (<https://avogadro.cc>) or Jmol (<http://jmol.sourceforge.net>). Animations corresponding to imaginary frequencies from vibrational analysis are provided as GIF files.

**Table S1.** Free energy calculations for solvents and methoxide ions

$$\text{Standard State Correction: } -0.593 * \ln[0.0409 / \text{Concentration}(M)]$$

Standard State Corrections (SSC) for Solvents					
	density (kg/m <sup>3</sup> )	Molar Mass	Conc. (M)	SSC (kcal/mol)	a.u.
CD3OD				1 No correction	-115.692696
CD3OD, neat	888	36.06	24.62562396	3.795444756	<b>-115.686647</b>
CD3OD in 1:1 v/v CD3OD: CD3OH	888	36.06	12.31281198	3.384408477	<b>-115.681254</b>
CD3OH				1 No correction	-115.689152
CD3OH, neat	867	35.06	24.72903594	3.797929765	<b>-115.683100</b>
CD3OH in 1:1 v/v CD3OD: CD3OH	867	35.06	12.36451797	3.386893487	<b>-115.677702</b>
<b>Calculation of free energy of solvation of methoxide ion in methanol solvent</b>					
$\Delta G(\text{MeO in Methanol}) = \Delta G(\text{MeO in Gas-phase}) + \Delta G(\text{solvation})$					
methoxide- <i>d</i> <sub>3</sub> , gas					-115.070323
methoxide- <i>d</i> <sub>3</sub> , solvated					-115.236854

**Table S2.** Isodesmic equations for the sequential reactions of complex **1** with 1:1 CD<sub>3</sub>OD : CD<sub>3</sub>OH (v/v)

<i>In 1:1 CD3OD: CD3OH</i>						$\Delta G$ (kcal/mol)
<b>1</b> + CD3OD (12.31 M) → <b>1-d1</b> + CD3OH (12.36 M)	-807.500847	-115.681254	→	-807.504023	-115.677702	<b>0.24</b>
<b>1-d1</b> + CD3OD (12.31 M) → <b>1-d2</b> + CD3OH (12.36 M)	-807.504023	-115.681254	→	-807.507293	-115.677702	<b>0.18</b>
<i>In neat CD3OD</i>						
<b>1</b> + CD3OD (24.6 M) → <b>1-d1</b> + CD3OH	-807.500847	-115.686647	→	-807.504023	-115.689152	<b>-3.56</b>

**Table S3.** Free energies corresponding to Scheme 5a in the manuscript

				SUM	REL (kcal/mol)	Notes
<b>Protonation of 1 with TfOD (strong acid)</b>						
<b>1 + TfOD</b>	-807.500847	-962.114077		-1769.614924	<b>0.0</b>	
<b>TS1</b>	-1769.609006			-1769.609006	<b>3.7</b>	Transition state for the direct protonation of the PtII-center of <b>1</b> without assistance from either ligand or solvent molecule
<b>Int1 + OTf<sup>-</sup></b>	-807.917152	-961.705091		-1769.622243	<b>-4.6</b>	Owing to a strong acid, formation of PtIV-D intermediate is exergonic

**Table S4.** Free energies corresponding to Scheme 5b in the manuscript

				SUM	REL (kcal/mol)	Notes
<b>Protonation of 1 with AcOD (weak acid)</b>						
<b>1 + CD3OD + AcOD</b>	-807.500847	-115.686647	-229.036193	-1152.223687	<b>0.0</b>	
<b>TS2</b>	-1152.183300			-1152.183300	<b>25.3</b>	Transition state for the protonation of the PtII-center of <b>1</b> with pseudoaxial assistance from solvent molecule
<b>Int2 + OAc<sup>-</sup></b>	-923.614710	-228.579508		-1152.194218	<b>18.5</b>	Owing to a weak acid acid, formation of PtIV-D intermediate is endergonic

**Table S5.** Free energies corresponding to Scheme 5c in the manuscript

				SUM	REL (kcal/mol)	Notes
<b>Protonation AFTER Hemiketal Formation</b>						
<b>1 + 2CD3OD + AcOD</b>	-807.500847	-231.373294	-229.036193	-1267.910334	<b>0.0</b>	
<b>TS3 + AcOD</b>	-1038.812705	-229.036193		-1267.848898	<b>38.6</b>	Transition State for the formation of hemiketal intermediate
<b>Int3 + CD3OD + AcOD</b>	-923.179946	-115.686647	-229.036193	-1267.902786	<b>4.7</b>	Owing to a strong acid, formation of PtIV-D intermediate is exergonic
<b>TS4 + CD3OD</b>	-1152.181889	-115.686647		-1267.868536	<b>26.2</b>	Protonation of the PtII-center by acetic acid; assisted by pseudoaxial coordination of hemiketal OD fragment
<b>TS5 + AcOD</b>	-1038.813660	-229.036193		-1267.849853	<b>38.0</b>	Direct Protonation of the Pt-CH3 bond

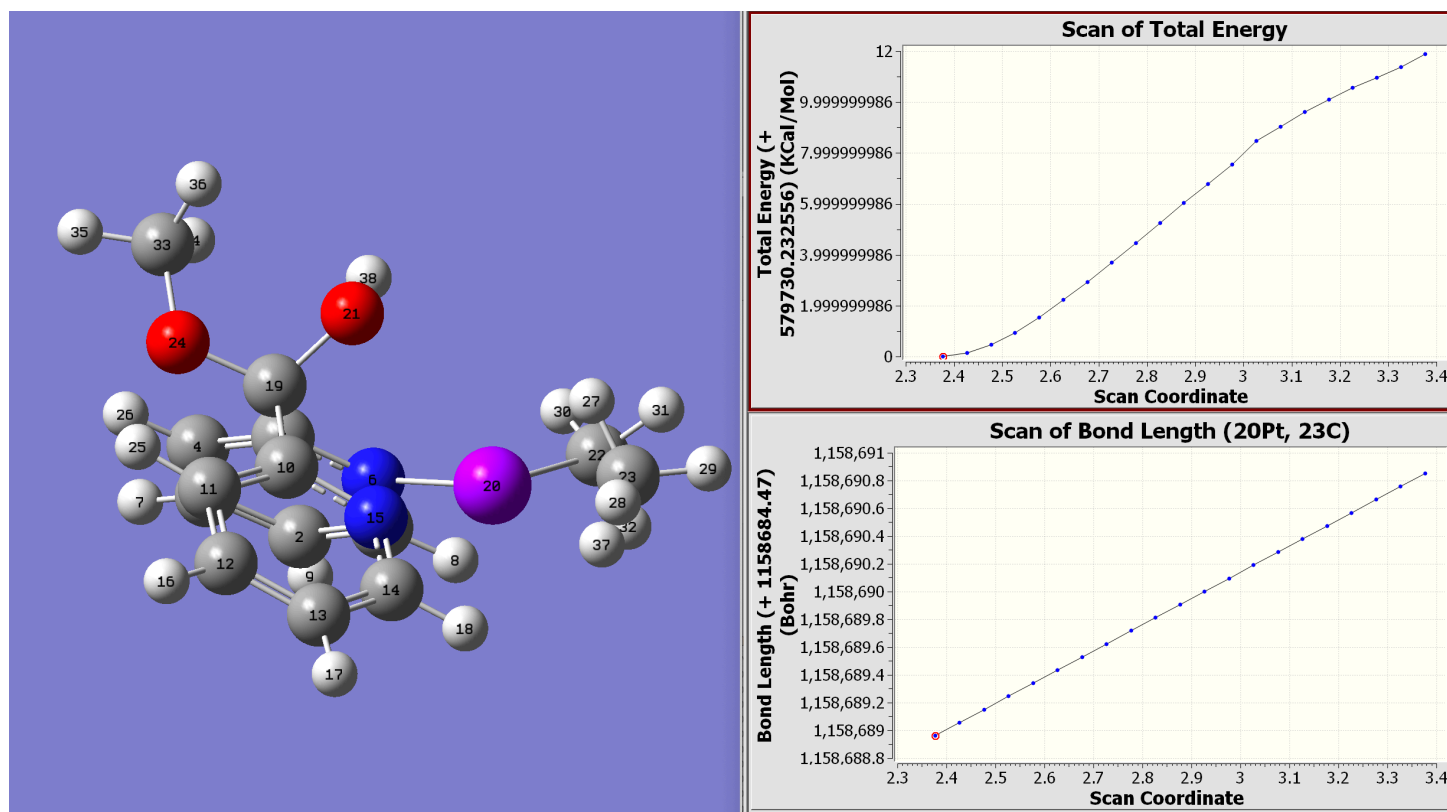
**Table S6.** Free energies corresponding to Scheme 6 in the manuscript (*rate determining step is highlighted in orange*)

	a.u.			SUM	REL (kcal/mol)	Notes
<b>1</b> + 2*CD3OD(neat)	-807.500847	-231.373294		-1038.874141	<b>0.00</b>	Starting Materials
<b>Int4</b> + CD3OD	-923.166479	-115.686647		-1038.853126	<b>13.19</b>	Formation of neutral 'hemiketalate' PtD intermediate
<b>TS6</b> + CD3OD	-923.139053	-115.686647		-1038.825700	<b>30.40</b>	Transition State for C-D reductive Coupling from Int1
<b>Int5</b> + CD3OD	-923.151644	-115.686647		-1038.838291	<b>22.50</b>	Zwitterionic sigma complex after reductive coupling
<b>Int6</b> + methoxide-d3(solvated)	-923.612110	-115.241797		-1038.853907	<b>12.70</b>	Formation of cationic 'hemiketal' Pt-D intermediate
<b>TS7</b> + methoxide-d3(solvated)	-923.599250	-115.241797		-1038.841047	<b>20.77</b>	<b>Transition State for C-D reductive Coupling from Int6</b>
<b>Int7</b> + methoxide-d3(solvated)	-923.615294	-115.241797		-1038.857091	<b>10.70</b>	Formation of cationic Pt-(D-CH3) sigma complex
<b>Int8</b> + methoxide-d3(solvated)	-923.615465	-115.241797		-1038.857262	<b>10.59</b>	Formation of cationic Pt-(H-CH2D) sigma complex
<b>TS8</b> + methoxide-d3(solvated)	-923.600469	-115.241797		-1038.842266	<b>20.00</b>	Transition State for C-H oxidative addition
<b>Int9</b> + methoxide-d3(solvated)	-923.612747	-115.241797		-1038.854544	<b>12.30</b>	Formation of 'hemiketal' Pt-H intermediate, isotopomer of <b>Int6</b>
TS9	-1038.798079			-1038.798079	<b>47.73</b>	Transition State for Associative Methane Loss
Int10 + CH3D	-998.404551	-40.468066		-1038.872617	<b>0.96</b>	Monomethyl PtII product, if methanolysis had occurred
<b>1-d1</b> + CD3OD(neat) + CD3OH(1M)	-807.504023	-115.686647	-115.689152	-1038.879822	<b>-3.56</b>	Formation of mono-deuterated product and release of 1M CD3OH

**Table S7.** Free energies corresponding to Scheme 7 in the manuscript (*rate determining step is highlighted in orange*)

	a.u.			SUM	REL (kcal/mol)	Notes
<b>First Deuteration of 1</b>						
<b>1</b> + 2*CD3OD(neat)	-807.500847	-231.373294		-1038.874141	<b>0.00</b>	Starting Materials
<b>TS7</b> + methoxide-d3(solvated)	-923.599250	-115.241797		-1038.841047	<b>20.77</b>	<b>C-D reductive coupling</b>
<b>TS8</b> + methoxide-d3(solvated)	-923.600469	-115.241797		-1038.842266	<b>20.00</b>	C-H oxidative addition
<b>First Protonation of 1-d6</b>						
<b>1-d6</b> + 2*CD3OH(neat)	-807.520221	-231.3662		-1038.886420	<b>0.00</b>	Starting Materials
<b>TS10</b> + methoxide-d3(solvated)	-923.613293	-115.241797		-1038.855090	<b>19.66</b>	C-D reductive coupling
<b>TS11</b> + methoxide-d3(solvated)	-923.612163	-115.241797		-1038.853960	<b>20.37</b>	<b>C-H oxidative addition</b>

**Figure S42.** Potential energy scan demonstrating gradual energy increase as a function of Pt(20)-C(23)H<sub>3</sub> distance of **Int7** (without a saddle point)



Energy (kcal/mol) scaled relative to **Int4**. Scan performed using modified redundant internal coordinates at the *m06/def2-tzvp* level with *smd* solvation in methanol

**Table S8.** Free energies for the reaction of **2** with CD<sub>3</sub>OD and AcOD (Scheme 8 in the manuscript)

Reaction of <b>2</b> with <b>X D</b> ( <b>X = OCD3</b> or <b>OAc</b> )	Notes	Complex	<b>X = OCD3</b>			<b>X = OAc</b>		
			XD = CD3OD	SUM	REL (kcal/mol)	XD = AcOD	SUM	REL (kcal/mol)
<b>2p + XD</b>	Complex <b>2</b> with OMe fragment exo to the PtII-center	-887.204933	-115.686647	-1002.891580	<b>0.00</b>	-229.036193	-1116.241126	<b>0.00</b>
<b>TS12 + XD</b>	TS for Ring-flip isomerization	-887.185963	-115.686647	-1002.872610	<b>11.90</b>			
<b>2 + XD</b>	Complex <b>2</b> with OMe fragment endo to the PtII-center	-887.203751	-115.686647	-1002.890398	<b>0.74</b>			
<b>TS13</b>	Transition State for PtII-protonation	X	X	X	X	-1116.209685	-1116.209685	<b>19.73</b>
<b>Int11 + X</b>	Cationic PtIV-D intermediate	-887.642370	-115.241797	-1002.884167	<b>4.65</b>			
<b>TS14 + X</b>	Transition State for C-D reductive Coupling from Int9	-887.629271	-115.241797	-1002.871068	<b>12.87</b>			
<b>Int12 + X</b>	Formation of cationic Pt-(D-CH3) sigma complex	-887.644831	-115.241797	-1002.886628	<b>3.11</b>	-228.596077	-1116.240908	<b>0.14</b>
<b>TS15 + X</b>	Transition State for C-H oxidative addition from sigma complex	-887.630441	-115.241797	-1002.872238	<b>12.14</b>			
<b>Int13 + X</b>	Cationic PtIV-H intermediate after C-H oxidative elimination	-887.643023	-115.241797	-1002.884820	<b>4.24</b>	-228.596077	-1116.239100	<b>1.27</b>
<b>TS16</b>	Deprotonation of the PtIV-H intermediate	X	X	X	X	-1116.210933	-1116.210933	<b>18.95</b>
<b>TS17 / TS17'</b>	Transition State for Associative Methane Loss	-1002.825087		-1002.825087	<b>41.72</b>	-1116.203112	-1116.203112	<b>23.85</b>
<b>2-d1 + XH</b>	Formation of mono-deuterated product and release of 1M CD3OH	-887.208151	-115.689152	-1002.897303	<b>-3.59</b>			

**Table S9.** Estimation of the barriers for Pt<sup>II</sup>-protonation of **2** and **2-d<sub>6</sub>** with AcOD (Scheme 9 in the manuscript)

Reaction of <b>2</b> with AcOD			SUM	Rel (kcal/mol)	
<b>2p + AcOD</b>	-887.204933	-229.036193	-1116.241126	<b>0.00</b>	
<b>2 + AcOD</b>	-887.203751	-229.036193	-1116.239944	<b>0.74</b>	
<b>TS13</b>	-1116.209685		-1116.209685	<b>19.73</b>	
					<b>kH/kD = 6.15</b>
Reaction of <b>2-d<sub>6</sub></b> with AcOH					
<b>2p-d<sub>6</sub> + AcOH</b>	-887.224283	-229.032649	-1116.256932	<b>0.00</b>	
<b>2-d<sub>6</sub> + AcOH</b>	-887.223073	-229.032649	-1116.255722	<b>0.76</b>	
<b>TS18</b>	-1116.227208		-1116.227208	<b>18.65</b>	

**Table S10.** Estimation of the barriers for Pt<sup>II</sup>-protonation of **2** and **2-d<sub>6</sub>** with CD<sub>3</sub>OD (Scheme 10 in the manuscript)

Reaction of <b>2</b> with CD3OD					
<b>2p + CD3OD</b>	-887.204933	-115.686647	-1002.891580	<b>0.00</b>	
<b>2 + CD3OD</b>	-887.203751	-115.686647	-1002.890398	<b>0.74</b>	
<b>TS14 + methoxide-d<sub>3</sub></b>	-887.629271	-115.241797	-1002.871068	<b>12.87</b>	
<b>TS15 + methoxide-d<sub>3</sub></b>	-887.630441	-115.241797	-1002.872238	<b>12.14</b>	
					<b>kH/kD = 1.73</b>
Reaction of <b>2-d<sub>6</sub></b> with CD3OH					
<b>2p-d<sub>6</sub> + CD3OH</b>	-887.224283	-115.683100	-1002.907383	<b>0.00</b>	
<b>2-d<sub>6</sub> + CD3OH</b>	-887.223073	-115.683100	-1002.906173	<b>0.76</b>	
<b>TS19 + methoxide-d<sub>3</sub></b>	-887.646794	-115.241797	-1002.888591	<b>11.79</b>	
<b>TS20 + methoxide-d<sub>3</sub></b>	-887.645593	-115.241797	-1002.887390	<b>12.55</b>	

## References:

- (1) Fulmer, G. R.; Miller, A. J. M.; Sherden, N. H.; Gottlieb, H. E.; Nudelman, A.; Stoltz, B. M.; Bercaw, J. E.; Goldberg, K. I. NMR Chemical Shifts of Trace Impurities: Common Laboratory Solvents, Organics, and Gases in Deuterated Solvents Relevant to the Organometallic Chemist. *Organometallics* **2010**, *29* (9), 2176–2179. <https://doi.org/10.1021/om100106e>.
- (2) Scott, J. D.; Puddephatt, R. J. Ligand Dissociation as a Preliminary Step in Methyl-for-Halogen Exchange Reactions of Platinum(II) Complexes. *Organometallics* **1983**, *2* (11), 1643–1648. <https://doi.org/10.1021/om50005a028>.
- (3) Zhang, F.; Broczkowski, M. E.; Jennings, M. C.; Puddephatt, R. J. Oxidative Addition Chemistry of Dimethyl(Dipyridyl Ketone)Platinum(II). *Can. J. Chem.* **2005**, *83* (6–7), 595–605. <https://doi.org/10.1139/v05-028>.
- (4) Barbasiewicz, M.; Małkosza, M. Intermolecular Reactions of Chlorohydrine Anions: Acetalization of Carbonyl Compounds under Basic Conditions. *Org. Lett.* **2006**, *8* (17), 3745–3748. <https://doi.org/10.1021/ol0613113>.
- (5) Monaghan, P. K.; Puddephatt, R. J. Oxidation of Dimethylplatinum(II) Complexes with Alcohols: Synthesis and Characterization of Alkoxoplatinum(IV) Complexes. *Organometallics* **1984**, *3* (3), 444–449. <https://doi.org/10.1021/om00081a019>.
- (6) Parkin, G. Temperature-Dependent Transitions Between Normal and Inverse Isotope Effects Pertaining to the Interaction of H–H and C–H Bonds with Transition Metal Centers. *Acc. Chem. Res.* **2009**, *42* (2), 315–325. <https://doi.org/10.1021/ar800156h>.
- (7) Sheldrick, G. M. SHELXT – Integrated Space-Group and Crystal-Structure Determination. *Acta Crystallogr. Sect. A Found. Adv.* **2015**, *71* (1), 3–8. <https://doi.org/10.1107/S2053273314026370>.
- (8) Sheldrick, G. M. Crystal Structure Refinement with SHELXL. *Acta Crystallogr. Sect. C Struct. Chem.* **2015**, *71* (1), 3–8. <https://doi.org/10.1107/S2053229614024218>.
- (9) Dolomanov, O. V.; Bourhis, L. J.; Gildea, R. J.; Howard, J. A. K.; Puschmann, H. OLEX2 : A Complete Structure Solution, Refinement and Analysis Program. *J. Appl. Crystallogr.* **2009**, *42* (2), 339–341. <https://doi.org/10.1107/S0021889808042726>.
- (10) Zhao, Y.; Truhlar, D. G. The M06 Suite of Density Functionals for Main Group Thermochemistry, Thermochemical Kinetics, Noncovalent Interactions, Excited States, and Transition Elements: Two New Functionals and Systematic Testing of Four M06-Class Functionals and 12 Other Function. *Theor. Chem. Acc.* **2008**, *120* (1–3), 215–241. <https://doi.org/10.1007/s00214-007-0310-x>.
- (11) Weigend, F.; Ahlrichs, R. Balanced Basis Sets of Split Valence, Triple Zeta Valence and Quadruple Zeta Valence Quality for H to Rn: Design and Assessment of Accuracy. *Phys. Chem. Chem. Phys.* **2005**, *7* (18), 3297–3305. <https://doi.org/10.1039/b508541a>.
- (12) Frisch, M. J.; Trucks, G. W.; Schlegel, H. B.; Scuseria, G. E.; Robb, M. A.; Cheeseman, J. R.; Scalmani, G.; Barone, V.; Petersson, G. A.; Nakatsuji, H.; Li, X.; Caricato, M.; Marenich, A. V.; Bloino, J.; Janesko, B. G.; Gomperts, R.; Mennucci, B.; Hratchian, H. P.; Ortiz, J. V.; Izmaylov, A. F.; Sonnenberg, J. L.; Williams, Ding, F.; Lipparini, F.; Egidi, F.; Goings, J.; Peng, B.; Petrone, A.; Henderson, T.; Ranasinghe, D.; Zakrzewski, V. G.; Gao, J.; Rega, N.; Zheng, G.; Liang, W.; Hada, M.; Ehara, M.; Toyota, K.; Fukuda, R.; Hasegawa, J.; Ishida, M.; Nakajima, T.; Honda, Y.; Kitao, O.; Nakai, H.; Vreven, T.; Throssell, K.; Montgomery Jr., J. A.; Peralta, J. E.; Ogliaro, F.; Bearpark, M. J.; Heyd, J. J.; Brothers, E. N.; Kudin, K. N.; Staroverov, V. N.; Keith, T. A.; Kobayashi, R.; Normand, J.; Raghavachari, K.; Rendell, A. P.; Burant, J. C.; Iyengar, S. S.; Tomasi, J.; Cossi, M.; Millam, J. M.; Klene, M.; Adamo, C.; Cammi, R.; Ochterski, J. W.; Martin, R. L.; Morokuma, K.; Farkas, O.;

- Foresman, J. B.; Fox, D. J. Gaussian 16 Rev. B.01. 2016.
- (13) Dennington, R.; Keith, T. A.; Millam, J. M. GaussView Version 6. 2019.
- (14) Marenich, A. V.; Cramer, C. J.; Truhlar, D. G. Universal Solvation Model Based on Solute Electron Density and on a Continuum Model of the Solvent Defined by the Bulk Dielectric Constant and Atomic Surface Tensions. *J. Phys. Chem. B* **2009**, *113* (18), 6378–6396.  
<https://doi.org/10.1021/jp810292n>.
- (15) Sparta, M.; Riplinger, C.; Neese, F. Mechanism of Olefin Asymmetric Hydrogenation Catalyzed by Iridium Phosphino-Oxazoline: A Pair Natural Orbital Coupled Cluster Study. *J. Chem. Theory Comput.* **2014**, *10* (3), 1099–1108. <https://doi.org/10.1021/ct400917j>.
- (16) Carvalho, N. F.; Pliego, J. R. Cluster-Continuum Quasichemical Theory Calculation of the Lithium Ion Solvation in Water, Acetonitrile and Dimethyl Sulfoxide: An Absolute Single-Ion Solvation Free Energy Scale. *Phys. Chem. Chem. Phys.* **2015**, *17* (40), 26745–26755.  
<https://doi.org/10.1039/c5cp03798k>.